The COLTRIMS Reaction Microscope—The Spyhole into the Ultrafast Entangled Dynamics of Atomic and Molecular Systems

Horst Schmidt-Böcking,* Joachim Ullrich, Reinhard Dörner, and Charles Lewis Cocke

Dedicated to Jan Peter Toennies on the occasion of his 90th birthday

The COLTRIMS Reaction Microscope C-REMI can image the momentum vectors of all emitted charged fragments in an atomic or molecular reactions similar to the bubble chamber in high energy particle physics. C-REMI can detect fragments with "zero" kinetic energy in an ultrahigh vacuum environment by projecting them with weak electromagnetic fields onto position-sensitive detectors. Geometrically a nearly 4π collection solid angle and a nearly 50% efficiency for a fivefold multi-coincidence can be achieved. Measuring time-of-flight and detector position the momenta of the fragments can be measured with excellent resolution (<0.01 a.u.; see A1 in the Appendix). Thus, multivector correlations in momentum space are measured, which provide insight into the entangled dynamics of atomic and molecular quantum systems. From these vector-correlations phases and energies can be deduced which allow for relative time measurements even in the zeptosecond range. C-REMI provides a "spyhole" into the secrets of ultrafast dynamics of atomic and molecular processes. It is applied today around the globe in numerous research projects in physics and chemistry. The purpose for writing this article is to demonstrate the universal application possibilities of C-REMI, and its high multi-coincidence efficiency and high momentum resolution. This paper will not give a review on all milestone experiments performed with C-REMI.

Prof. H. Schmidt-Böcking, Prof. R. Dörner
Institut für Kernphysik
Goethe Universität Frankfurt
Max von Laue Str.1, 60438 Frankfurt, Germany
E-mail: hsb@atom.uni-frankfurt.de

Prof. J. Ullrich
PTB
38116 Braunschweig, Germany

Prof. C. L. Cocke
Department of Physics
Kansas State University
Manhattan, KS 66506, USA

The ORCID identification number(s) for the author(s) of this article can be found under https://doi.org/10.1002/andp.202100134

1. Introduction

Progress in understanding physical phenomena is achieved both by developing new theoretical concepts and by inventing novel experimental instrumentation. Such a novel experimental approach represents the COLTRIMS Reaction Microscope C-REMI,[1–3] providing the possibility to visualize the collective motion of electrons and nuclei in a single reaction process. By multifragment coincidence detection of electrons and nuclei and measuring their momenta with subatomic resolution (see A2 in the Appendix) the "possibly collective motion," i.e., the "dynamics," of all involved electrons and nuclei in a single-event reaction process can be explored with atto- and even zeptosecond time resolution. It is important to notice that in each single event measurement the dynamics of all involved particles must be "collective and entangled" since for this single event the total momentum and angular momentum are conserved.

Quantum phenomena, like particle-wave dualism, the stability of atoms, contributions of virtual photons to the energy of eigenstates, and collective electron dynamics in atoms and molecules are at variance with the laws of classical physics, according to which, fast moving electrons inside atoms should emit radiation and permanently undergo collisions with each other, yielding a high degree of self-ionization. Atoms ought to collapse or to explode within femtoseconds into many fragments, and stable atoms could not exist. Since Bohr's postulates[4] and the ensuing development of the quantum theories of Heisenberg[5] and Schrödinger[6] (which describe stationary properties of atoms), most physicists have been satisfied with this theoretical explanation and accept that quantum physics is established and differs dramatically from classical physics.

Nevertheless, the question is tempting, whether the theoretical description by Heisenberg and Schrödinger and their successors, who added relativistic effects and QED, is the final truth and sufficient to completely understanding the properties of such quantum objects. Is it, regardless of the great success of quantum

**ADVANCED
SCIENCE NEWS**
www.advancedsciencenews.com

annalen
der **physik**
www.ann-phys.org

theory, a meaningful question how the electrons move inside an atom with respect to each other? Such speculative issues could potentially be addressed if we had an approach to visualize the motion of electron pairs or even parts of the total electronic shell inside atoms or molecules at a given time. This paper aims to describe an experimental approach that probably enables the investigation of such questions.

From Compton scattering it is known that the electrons inside atoms exhibit a momentum distribution. By performing a coincidence between the scattered photon and the ejected electron, the momentum of a single electron inside an atom can be measured.[7] In agreement with theory, measurements yield continuous momentum distributions for ejected electrons. The momentum vector-sum of all electrons plus the nucleus' momentum-vector, however, adds up to exactly zero in the center-of-mass system at any time. Since the electron positions and the forces between them are not localized in strict classical sense, we expect that all electrons move together in a well-ordered manner.

For the remainder of this paper we call this "ordered collective motion" of all electrons as a function of time "entangled." We borrow the term from quantum mechanics but use it in a broader sense. Most relevant for the processes discussed here are momentum and angular momentum conservation which are satisfied at any moment in time. Angular momentum plays a particular role in this context as spin angular momentum has no counterpart in classical physics. For stationary eigenstates, standard quantum theory makes no prediction how the collective motion of all constituents inside atoms and molecules varies as a function of time. In reactions between quantum particles, however, motion and its variation with time plays a key role. Therefore the visualization of such reactions is a main topic of this paper, too.

To explore the relative motion of electrons inside atoms or molecules, the experimenter must multiply ionize (see A3 in the Appendix) the object at a given instant of time and measure the momenta of all emitted electrons in coincidence. Performing such a multifragment coincidence measurement in atomic physics requires a detection approach, where the emitted electrons and ionic fragments can be detected with high multicoincidence efficiency and excellent subatomic momentum (kinetic energy) resolution even if they have practically zero kinetic energy.

Considering the time scale of the ultrafast motion of electrons inside atoms the time of an electron "revolution" around the nuclei amounts to a few tenths of attoseconds. How can such an ultrafast collective process be explored experimentally? To visualize such fast dynamics, a relative time resolution of atto- or even zeptoseconds is required. Presently laser based ultrafast pump and probe methods (P&P)[8] can hardly provide such a time resolution. However, zeptosecond time resolution can be achieved by measuring the momentum vectors of several fragments emitted in one reaction in coincidence. From the relative vector orientations, phase differences, and thus relative time differences can be deduced.

The measurement of the motion of electrons and nuclei in atoms or molecules has always been a key issue in quantum physics. Heisenberg proposed in his famous 1927 paper[9] the concept of electron-position measurement using a so-called γ-microscope (see A4 in the Appendix) to obtain information on the electron motion inside an atom. Schmidt-Böcking et al.[7] show that positions of single electrons at a given instant of time, however, can never be measured with subatomic resolution and thus by using Heisenberg's γ-microscope no information on the electron motion can be obtained. The microscope approach for measuring positions is based on the Fourier transformation of a momentum distribution of a larger ensemble of events.

Fortunately, this is not true for momentum measurements of electrons and nuclei in a single event. As presented by Schmidt-Böcking et al.[7] the momenta of quantum particles can indeed be measured in a single event with "ultimate" resolution. This is due to the facts that, first, the total momentum of the reaction partners in the initial state can be prepared with very high (i.e., subatomic) precision and that, second, this total momentum is conserved during the time period of a measurement. Consequently a "microscope" for the observation of inner atomic or molecular reaction dynamics must be designed as a momentum, rather than as a position spectrometer. The C-REMI[1–3] is a multiparticle imaging device where by performing a multiparticle coincidence experiment the complete entangled dynamics of quantum systems can be visualized.

2. Physical Features of the C-REMI Detection Device

Besides these considerations on the principles of a quantum measurement there are provisions to satisfy for the practical performance of a high-resolution momentum measurement. To yield excellent subatomic momentum resolution in a quantum measurement, the experimenter has to carefully prepare the momenta of the projectiles and the target atoms in the initial state (very shortly before the reaction). The overall obtained precision can never be better than the precision of the initial-state preparation. An optimal preparation of the initial-momentum state requires to cool down the random motion of the colliding projectiles and target atoms or molecules. This can be done by either using a supersonic gas jet or a magneto optical trap. Furthermore by geometrical collimation of the projectile beam with slits (see **Figure 1** example for an ion beam) or of the target supersonic jet by using skimmers, one can indeed achieve subatomic momentum precision in the transverse direction.[10,11]

Furthermore a multifragment coincidence detection system requires the use of modern position-sensitive detectors with appropriate electronical readout, that measure the impact position but also the time of impact. From the measured time of impact the experimenter knows which fragments belong to the same reaction. Using timed-bunched projectile beams, the time-of-flight (TOF) from the instant of the reaction to the impacts on the detector is known for each fragment. From this TOF parameter the momentum can be determined for each fragment.[1,2] Such a TOF approach yields even better resolution when the fragments kinetic energy, i.e., their velocity, is lower. In this case the TOF increases and the relative resolution of the measured momentum is improved, since the time resolution of the detector remains constant. Thus, for an electron moving with, e.g., 10^{-2} a.u. velocity (kinetic energy about 1.3 meV) and for a distance of 20 cm from the reaction location to the detector, the electron TOF can approach 1 μs, if no extraction voltage is applied. The typical time
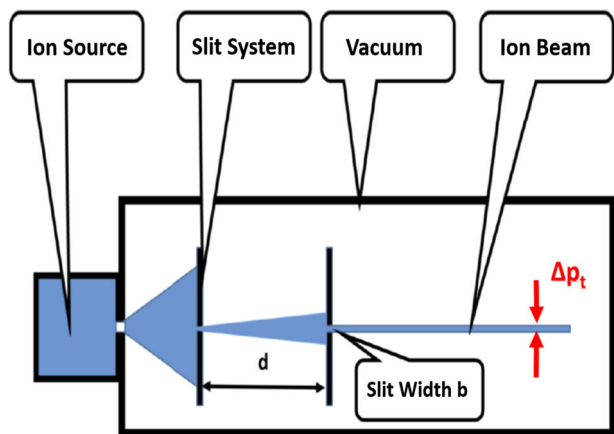
**ADVANCED
SCIENCE NEWS**

www.advancedsciencenews.com

annalen
der **physik**

www.ann-phys.org

Figure 1. Scheme of a macroscopic collimation approach to achieve sub-atomic transverse momentum resolution.[3,7]
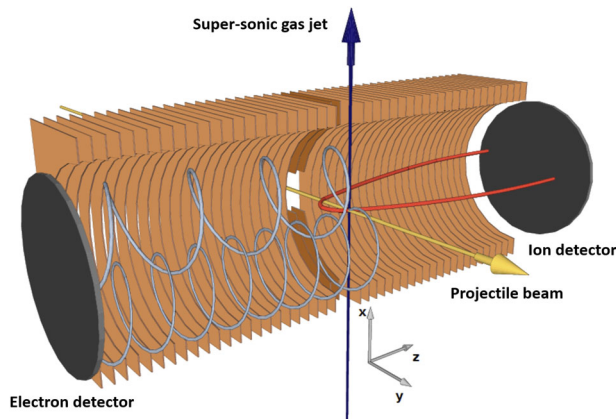

Figure 2. C-REMI spectrometer set-up with examples of electron and recoil ion trajectories (gray and red lines). The electric field is applied by connecting the brown copper sheets to properly set static voltages, the magnetic field by Helmholtz coils (not shown here).[12]

resolutions of about 100 ps correspond to a relative momentum resolution below 10^{-3}. Thus an electron energy resolution in the micro-eV range can be obtained.

Some of the experiments address the reaction induced by the impact of ions delivered from a particle accelerator. For this case of experiments it is of great advantage if the momentum of the recoiling target ion is measured instead of the very small momentum change of the scattered projectile. For the target ion, since it was nearly at rest in the laboratory system before the collision the momentum change is relatively large and can be measured in so-called "inverse kinematics" with high precision. To illustrate which improvement in resolution can be obtained by measuring in the "inverse kinematics" approach, the energy loss ΔE measurement of a 10 MeV proton ionizing a He atom is considered

$$10 \text{ MeV p} + \text{He} \rightarrow \text{p} + \text{He}^{1+} + \text{e} \, (\Delta E) \qquad (1)$$
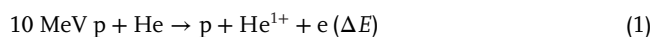
If the experimenter would measure ΔE by detecting the momentum vectors of the proton in the initial and final state the typically achievable resolution would be worse than a few hundred eV, because of experimental limitations in momentum-state preparation and momentum measurement of the fast proton. In "inverse kinematics" one rather measures the sum of the kinetic energies of electron and recoil ion in the final state. The kinetic energy of the emitted electron can be measured with about 1 meV resolution. Using a supersonic jet as target, the He atom velocity before the reaction is known with an accuracy of about 20 m s^{-1}. In a typical large impact parameter collision the final-state recoil momentum is commonly in the order of a few a.u. Thus the recoil kinetic energy can also be measured with about 1 meV energy resolution by using C-REMI. Therefore, using this "inverse kinematic" approach the relative resolution in the energy loss measurement ΔE can be better than 10^{-8} or even 10^{-10} with respect to the kinetic energy of the projectile, which is about four to five orders of magnitude improvement compared to the case of fast projectile detection.

In **Figure 2** the scheme of a C-REMI set-up is shown.[12] A well-collimated projectile beam (ions, electrons, photons from synchrotron photon sources, laser beams, etc.) collides in ultrahigh vacuum (typically below 10^{-9} Torr) with a well-collimated cold su-

personic gas jet. In the tiny intersection region (typically smaller than 1 mm³ volume) the reaction (ionization, charge transfer, fragmentation, etc.) occurs. The designed electric field configuration is achieved by applying the proper voltages to each copper electrode (brown sheets in Figure 2) thus optimal time and space focusing is ensured.[1,2] The static magnetic field (coaxial direction) is applied by Helmholtz coils (see **Figure 3**). The applied magnetic field prevents that the ejected higher energetic electrons do escape. Thus also for those electrons a nearly full detection efficiency is obtained. The projectile beam and the gas jet are dumped downstream of their flight path. The reaction zone is inside a momentum spectrometer, where well-designed static electric and magnetic fields are applied. Thus all charged fragments are projected on two position-sensitive detectors, which are mounted in opposite direction to each other perpendicular to the projectile beam direction.

The initial momentum of each fragment (the fragment momentum immediately after the reaction) is determined from the measured TOF and the positions of the intersection zone (known with better than 1 mm precision) and impact on the detector.[1,2] Knowing the applied spectrometer fields, the trajectory of the fragment inside the spectrometer and thus the initial momentum can then be deduced.[1,2] The spectrometer fields must be designed such that the trajectory is unambiguous.

Spectrometers with an extraction perpendicular to the ion beam are very suitable when the projectile beam is always travelling exactly the same path and when the beam width is small compared to the spacing of the copper electrodes (beam width typically a fraction of a mm). In case of perpendicular extraction, the static electric field is generally symmetric with respect to the spectrometer axis. The electrodes are mounted as a chain of copper rings in short distances to each other to ensure that possible outer electric fields are very well shielded.[1–3]

Depending on the kind of experiment, the optimal direction of the extraction with respect to the projectile beam direction may alternatively be parallel to the ion beam direction. In Figure 3, a C-REMI spectrometer is shown,[1] which allows to choose the direction of extraction parallel to the beam or even in any other direction. This C-REMI was designed for experiments inside an
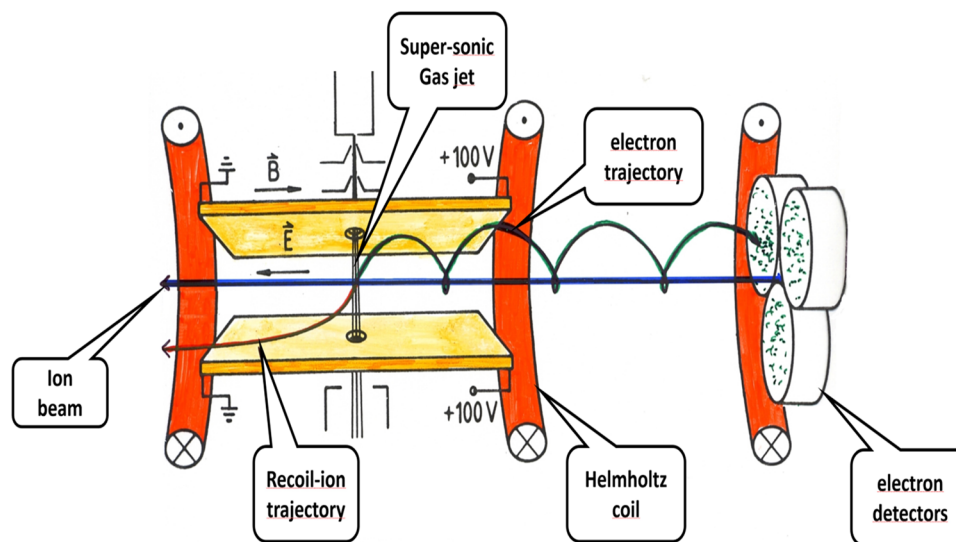
Figure 3. C-REMI spectrometer installed in ion storage rings.[1a,c,d,e]

ion-beam storage ring where the position of the passing beam varies during the beam accumulation in the storage ring. Thus a wide opening for the ion beam inside the spectrometer is required. Details on this setup can be found in the papers of Ullrich and co-workers.[1a,c,d,e]

As already stated to achieve the required excellent momentum resolution, the initial momenta of the collision partners (projectiles as well as target) must be prepared with the same or even better momentum precision. In Figure 1 the scheme of the preparation of the projectile transverse momenta is shown. To prepare the target atoms in a momentum state with subatomic precision, the formation of the gas target as supersonic jet[10,11] can yield the required precision. In **Figure 4** (upper part) the scheme of a supersonic jet device is shown.

Depending on the required pressure in the interaction chamber, the pressure reduction from the first stage (typically 10^{-3} Torr range) to the region of intersection can be achieved by one and more skimmer steps separating different pumping stages. The width of the velocity distribution of the atoms or molecules in the gas jet strongly shrinks compared to the thermal Maxwell–Boltzmann velocity distribution[11] (see Figure 4 lower part). For a typical half width of the velocity distribution of about 20 m s^{-1} this would yield an uncertainty in momentum of about 10^{-3} a.u. or in kinetic energy spread about 0.3×10^{-9} a.u. or 8×10^{-9} eV for the case of helium. The achievable momentum spread depends on the atomic or molecular target species. Some experimental groups have successfully used a cloud of atoms in a magneto-optical trap as target, which provide the ultimate limit of target cooling.[13]

To perform a multifragment coincidence measurement with the above described C-REMI approach, one needs detectors with multihit capability. As described by Jagutzki et al.[14] multichannel plate detectors can detect charged fragments with practically zero kinetic energy since the fragments can be post-accelerated just before the detector and thus induce electron avalanches in the detector's microtubes such that the event becomes electronically detectable. The impact position and impact time of each

fragment on these detectors can be measured by collecting the electron avalanche, e.g., with delay-line anodes (see **Figure 5**). As described by Ullrich and co-workers,[1–3] these anodes (or other position-sensitive anode structures[12,14]) can simultaneously detect several fragments resulting from the same reaction process. For each fragment up to seven time signals are electronically registered and stored event after event in "List Mode"[3] in a computer. In **Figure 6** a complete C-REMI system is shown.[15]

In this way the experimenter produces a list of a huge number of events, where each event contains full information on the momenta of all emitted fragments in this event. In essence the experimenter stores a movie of the entire experiment, which can be replayed over and over again with different analysis conditions of the measured data.

In summary, the following requirements are important for high-resolution multifragment momentum imaging.

a) The overall multicoincidence detection efficiency ϵ must be as high as possible. Therefore all charged fragments are focused by electromagnetic fields on the two detectors mounted in opposite directions (see Figure 2). The superimposed magnetic field ensures that also electrons up to keV kinetic energy are projected on the detector. Furthermore the single fragment detection efficiency $\epsilon1$ of the channel-plate detector must be as large as possible., e.g., if the single fragment efficiency is $\epsilon1 = 0.9$ we obtain for a fivefold coincidence $\epsilon5 = (\epsilon1)^5$ with $\epsilon5 = 0.59$ and in case of $\epsilon1 = 0.5$ we obtain for $\epsilon5 = 0.031$. This is nearly a factor of 20 difference in efficiency.

b) As outlined above the achievable momentum resolution depends on the projectile and target momentum preparation (cooling), but also on the length of the fragment trajectory in the spectrometer.

3. Benchmark Experiments

During the last three decades the availability of C-REMI enabled numerous milestone observations in physics and chemistry. To
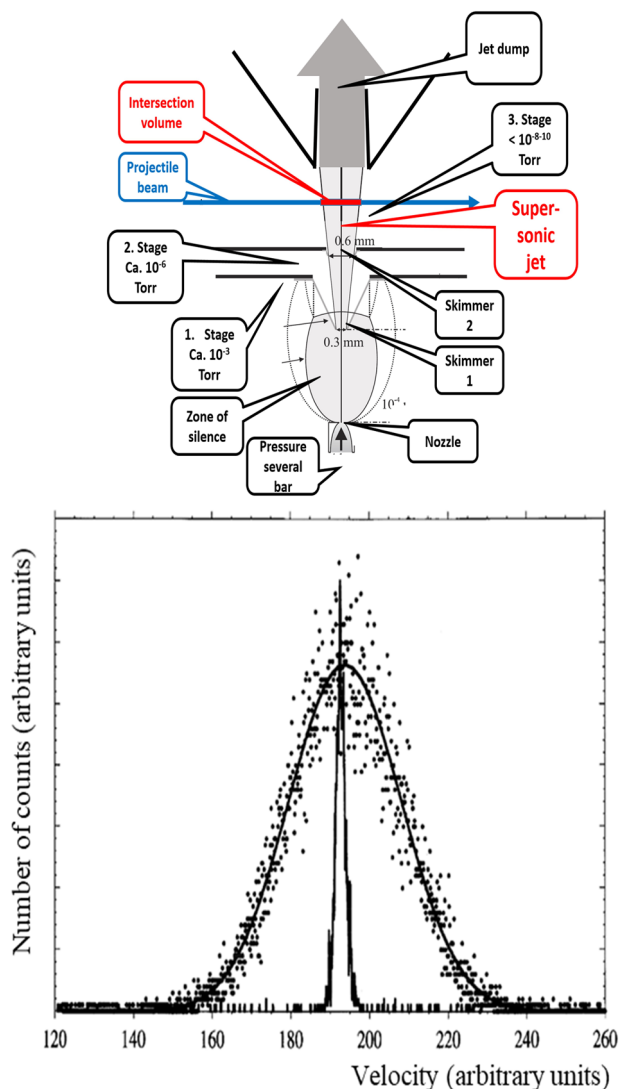
**ADVANCED
SCIENCE NEWS**

www.advancedsciencenews.com

annalen
der **physik**

www.ann-phys.org

Figure 5. Left: delay-line anode structure. Right: complete delay-line detector with microchannel plates (black area) and holder.[14]

Figure 6. C-REMI system of the Frankfurt group mounted at the European XFEL.[15]

Figure 4. Upper part: scheme of supersonic gas jet formation.[11] Lower part: comparison of measured velocity distribution of a warm diffusive gas jet (dots) and of a cooled supersonic gas jet (narrow distribution).

cite all here would go beyond the scope of this short review article. Therefore a short selection is listed and discussed here. This selection contains mainly experiments to which the authors themselves did contribute. We apologize for not discussing important discoveries of other groups achieved with C-REMI.

We have chosen the following experiments:

1) ultrahigh resolution of Q-value or energy loss measurement,
2) experimental observation of kinematical properties of so-called "virtually existing" off-shell states,
3) Einstein's double slit experiment—investigated by Young-type interference structures in slow H_2^+ + He collisions,
4) visualization of directional quantization of quasi-molecular orbitals in slow ion–atom collisions,
5) direct observation of the H_2^+ vibrational wave function in momentum space,
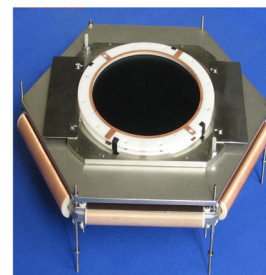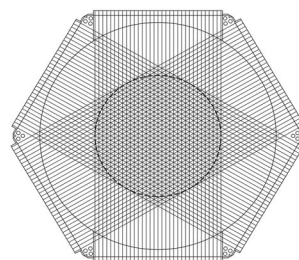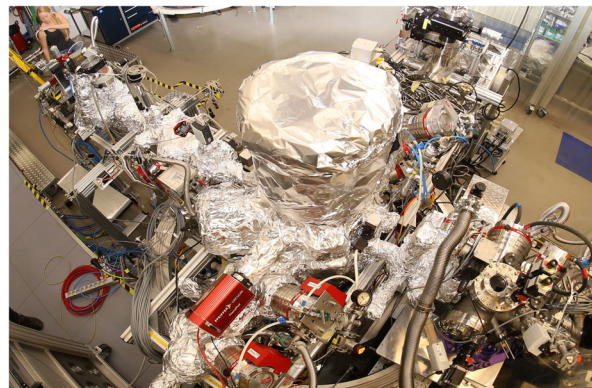
6) experimental separation of He ionization in the photo- and Compton effect,
7) multiphoton processes—experimental verification of the rescattering mechanism,
8) multivector correlation measurements in molecular fragmentation processes- search for dynamical symmetry breaking and observation of aligned very short-living exotic states,
9) single photon-induced interatomic Coulombic decay,
10) laser pump and probe measurements,
11) structure of the He-trimer Efimov state,
12) imaging of structural chirality, and
13) zeptosecond time-resolving studies.

3.1. Ultrahigh Resolution Q-Value or Energy Loss Measurement

The group of Ullrich and Moshammer[16,17] demonstrated the high-resolution power of C-REMI in measuring energy losses and Q-values as well as tiny deflection angles to explore the ionization dynamics in high-energy ion–atom collisions. They investigated the He single ionization in collisions with 100 MeV/u C^{6+} (total projectile kinetic energy $E_{pkin} = 1200$ MeV, projectile velocity $v_p = 63$ a.u., projectile momentum $p_p = 1.39 \times 10^6$ a.u.) and with 3.6 MeV/u Au^{24+}, respectively, 3.6 MeV/u Au^{53+} on He ($E_{pkin} = 709$ MeV, $v_p = 12$ a.u., $p_p = 4.3 \times 10^6$ a.u.).[16] Using the traditional method of measuring the final kinetic energy of the scattered projectiles the very small energy losses of typically 100 eV or even much lower and the tiny deflection angles would never be detectable. Using C-REMI, however, the energy loss and the details of the ionization process could be visualized with orders
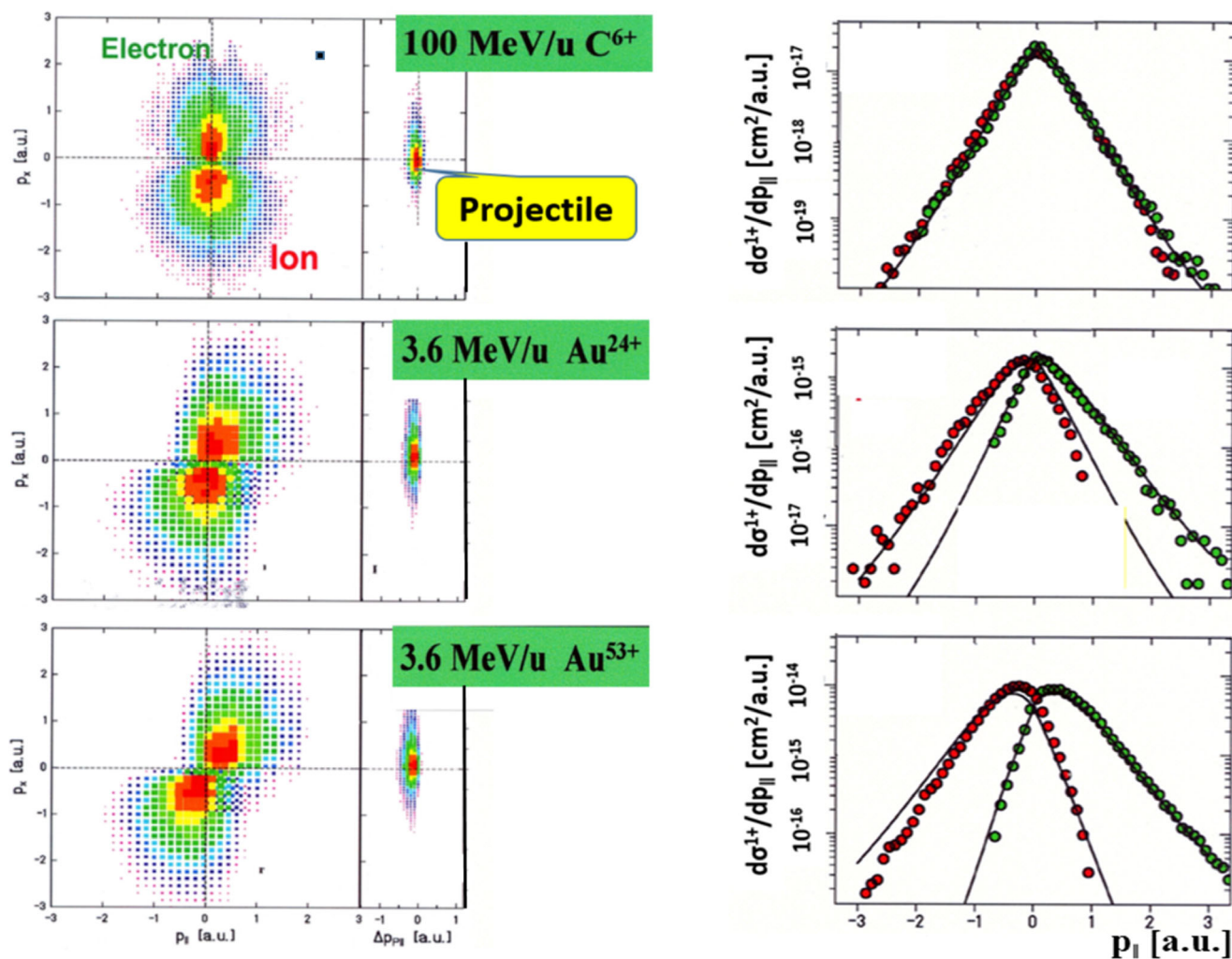
Figure 7. Electron and recoil-ion momentum distribution of He single-ionization measured in coincidence for the three indicated fast projectile-atom collision systems. The resulting projectile momentum change is calculated event by event as sum of electron and recoil-momentum vector. In the right column the distributions of the longitudinal momentum components of electron and recoil are shown. On the abscissa the longitudinal components of the electron and recoil ion are plotted in a.u.[16,17] The initial projectile momenta are 1.4×10^6 a.u. for the C beam and 4.6×10^6 a.u. for the Au beam.

of magnitude improved resolution, since the kinetic energies of the emitted electrons and recoil ions (i.e., measuring in inverse kinematics) as well as the recoil charge state (i.e., knowing the degree of ionization and thus the ionization energy) were precisely measured.

In **Figure 7** (left column) fully differential momentum distributions measured event after event for electrons (upper part), for recoil ions (lower part) and in the middle column for the projectile ion (sum of electron and recoil ion momentum vector) are plotted. The upper limit of the error bars for the momentum measurement is below 0.1 a.u. (see size of black square in most upper part of Figure 7 left column). Since for all three collision systems the projectile momentum is larger than 10^6 a.u. this detection approach provides a relative resolution in momentum exchange and energy-loss measurement of below 10^{-7}.

The measured momentum distributions of electron and recoil ions show a dipole distribution like in photoionization. For the fastest projectile velocity and lowest ion charge the electron and recoil momenta are emitted perpendicular to the ion path and their momenta are nearly balancing each other. Thus the projectile momentum change is even smaller than the electron or recoil ion momenta and much smaller than the momentum spread of the incoming ion beam. Therefore the projectile does not provide the large electron and recoil momenta. These electron and recoil momenta are already present in the initial He-ground state. Rather the virtual photon field (with a broad energy distribution) created by the projectile provides only the ionization energy but not the momentum change. With increasing projectile charge the postcollision interaction between projectile and electron as well as recoil ion increases thus the electron emission turns slightly forward and the recoil emission backward. This interpretation is supported by theory (solid lines in left part of Figure 7).[16,17] Direct binary encounter ionization is not visible in the data.
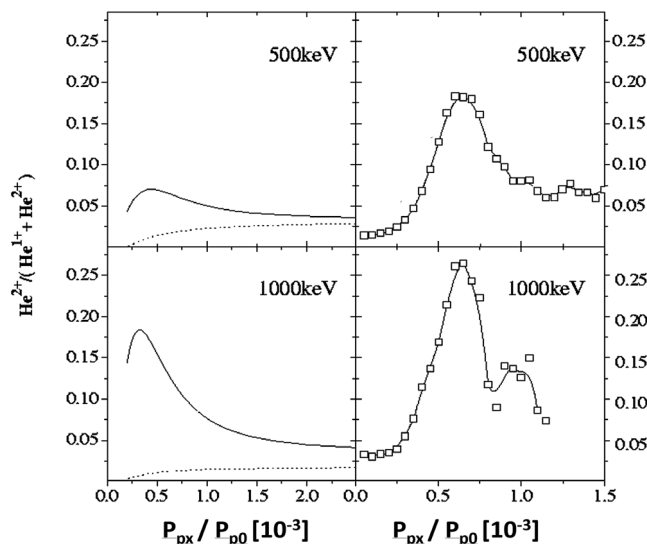
Figure 8. Ratios of transfer ionization to capture probabilities (left column theory by Kheifets[20] and right column experimental data by Mergel,[19] see text).
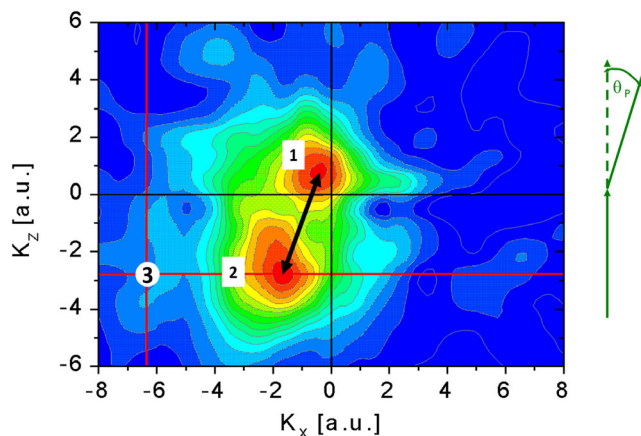

Figure 9. He^{2+} recoil-ion momentum distribution in the nuclear scattering plane for the transfer ionization process 1 MeV Proton projectiles on He.[19] Right: The direction of the H° deflection. The H° scattering angle θ_p is 0.55 mrad. The kinetic energy difference of the recoil ions between the two peaks 1 and 2 is about 65 meV. The momentum resolution is about 0.1 a.u. and thus the recoil energy resolution about 1 meV.[19]
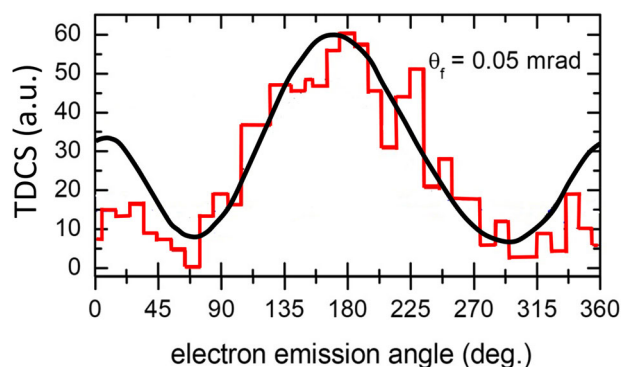
3.2. Experimental Observation of Kinematical Properties of Non-s^2 Contributions in the He Ground State

The He ground state energy can be calculated with high precision in a multiconfiguration approach.[18] In this approach also non-s^2 contributions are taken into account like p^2, d^2, etc. off-shell contributions. The calculation yields about 98% s^2 and 1% p^2 contributions.[19,20] The strength of such contributions was so far indirectly determined from high-precision photon energy spectroscopy. It is shown here, that such contributions can also be explored by high-resolution momentum measurements in fast proton on He transfer ionization processes.

The transfer ionization measurements described here were already performed in the early nineties. In fast proton on He collisions (0.3 till 1 MeV proton impact energy) the transfer ionization process[19–23]

$$p + He° \rightarrow H°^+ + He^{2+} + e \qquad (2)$$

was measured using the C-REMI approach by a recoil ion scattered H° coincidence. At lower impact energies capture of one electron and ionization of the second electron mainly proceeds via uncorrelated processes where the second electron is mostly ejected by interaction with the projectile Coulomb field. The ejected electron momentum and thus also the recoil-ion momentum show at lower energies a broad uncorrelated momentum distribution. With increasing projectile energy this uncorrelated reaction channel strongly decreases and it was expected that the "classical" Thomas processes would yield the dominant contributions.[19,24] In **Figure 8** for 500 and 1000 keV proton energy the ratios of transfer ionization to capture probabilities are plotted as function of the H° transverse momenta p_{px}, left column theoretical calculations by Kheifets and co-workers[20] and right column experimental data by Mergel et al.[19] The solid line includes s^2 and non-s^2, the dotted line only s^2 contributions. In agreement with the data the ratio peaks near to 0.5 mrad scat-

Figure 10. Measured triple differential cross-sections (red solid line) of transfer ionization in 630 keV on He collisions and 20 eV kinetic energy of the electron corresponding to maximum two (Figure 9) for the projectile scattering angle of 0.05 mrad. The black solid line is the theoretical prediction for the non-s^2 contributions. Theory and experiment are relatively normalized.[21,22]

tering angle and increases with increasing proton energy. After integration over the total solid angle of 4π more than 90% of the total cross-section comes from the impact parameter region corresponding to 0.5 mrad. Before these measurements were performed it was generally accepted that the main contribution to the total cross-section was due to the Thomas processes.

The original goal of the measurement was to investigate the kinematical details of these classical (e–e)- and (e–N)-Thomas-capture processes.[24] These processes should show a characteristic momentum pattern for the recoil ions. The with C-REMI measured data, however, unexpectedly gave evidence that beside the Thomas processes also transfer ionization occurred via such non-s^2 contributions (**Figure 9**). The experiment together with theory[19–23] provided evidence (see **Figures 9** and **10**) that such contributions can be visualized by the recoil ion momentum patterns measured in a multiparticle coincidence by using the high-resolution C-REMI approach.

**ADVANCED
SCIENCE NEWS**

www.advancedsciencenews.com

annalen
der **physik**

www.ann-phys.org

In the (e–e)-Thomas-capture process the projectile nucleus passes the He atom at very large impact parameters and scatters on one bound He target electron in a binary collision under 45° with respect of the projectile flight path. On its further path the kicked electron can collide in a subsequent binary process with the other He electron, thus electron 1 can be scattered under 0° and the other electron 2 is then ejected under 90° into the continuum. This forward moving electron 1 (its velocity vector matches in this case with the projectile velocity) is then captured by the parallel moving projectile. This e–e-collision process yields He-double ionization. The He^{2+} recoil remains as a spectator and thus its final momentum is close to zero. This billiard like two-step process requires that the projectile is deflected under the angle of $\theta_p = 0.55$ mrad. The peak number 1 in Figure 9 can unambiguously identified as contribution of the classical (e–e)-Thomas-capture process.[19,24] From the momentum distribution of peak 1 (position and its width) one can deduce that at 1 MeV impact energy the recoil ion projectile interaction (perturbation) is very weak (the transferred kinetic energy between the nuclei is below 10 meV compared to 1 MeV proton impact energy). This information is important for the analysis of the momenta in peak 2.

In case of the so-called nuclear (e–N)-Thomas process the projectile interacts with electron 1 which is then scattered on the He nucleus into forward direction (about 0°) and subsequently captured by the proton. Electron 2 is kicked-out by a noncorrelated projectile perturbation process. In this process the He recoil receives a high transverse momentum of about 6.4 a.u. and should show up at location 3. The data in Figure 9 show, however, that the contribution of the (e–N)-Thomas process at 1 MeV proton energy is not observable in this channel of the production of doubly charged He ion.

In Figure 9 a second strong maximum (peak 2) appears at $p_{recz} = -2.8$ a.u. and $p_{recx} = -1.8$ a.u. indicating there must be another, so far, unconsidered mechanism (the non-s^2 contribution channel) enabling transfer ionization at $\delta_p = 0.55$ mrad. The analysis of the momenta corresponding to peak 2 showed that electron 1 is captured at large impact parameters into the H^{0+} ground state (Brinkmann Kramer mechanism) and the second He electron 2 is emitted backward under about 135° (a narrow angular cone) with a high momentum of ≈4 atomic units (i.e., about 220 eV kinetic energy). Mergel et al.[19] found that the total cross-section for this maximum follows a $v_p^{-7.4}$ law, whereas the Thomas process follows a v_p^{-11} law. Peak 2 is the dominant transfer ionization channel at higher projectile velocities.

What is the mechanism behind this high energetic and directed electron 2 emission and the quite localized position of recoil ion momenta (peak 2) in the x–z-recoil ion momentum plane? We try to provide evidence here that this highly correlated momentum pattern can only be due to highly correlated momentum structure in the initial He ground state. First we analyze the transverse (x-direction) of the recoil momenta. The projectile transverse momentum $p_{H°x}$ for the scattering angle $\theta_p = 0.55$ mrad is $p_{px} = +6.4$ a.u. for each scattered H°. Thus if this projectile deflection were only due to a projectile–recoil interaction the recoil ion momentum would have to balance this and should be $p_{recx} = -6.4$ a.u. However, this is in clear discrepancy with the experimental observation. Since the complete momentum balance of the (H°–He^{2+}–e) system was measured for each single event,

the experimenter knows that the missing transverse momentum of about 4 a.u. is taken away by the ejected electron 2. Because the perturbation by the projectile is rather weak, as we know from the analysis of peak 1, this directed momentum of electron 2 of about 4 a.u. cannot result from a possible uncorrelated projectile–electron 2 interaction. Thus it must be a property of the correlations in the He initial state wave function.

This conclusion is supported also by the analysis of the measured momenta in z-direction (direction of projectile impact). At very large impact parameters electron 1 can only be captured into the H° ground state, if electron 1 in its initial state is moving at the instant of capture with the projectile velocity in z-direction, i.e., its p_z momentum is 6.4 a.u. Since the He atom was at rest in the laboratory system at the instant of the reaction, the momentum vector of the remaining recoiling He^{1+} ion must be $p_{He1+z} = -6.4$ a.u. The experimental observation shows that in all these capture processes the He^{1+} recoil ions instantly fragment into a free electron 2 and the recoil ion He^{2+}. Thus the observed characteristic momentum pattern of peak 2 must be only due to the initial momentum correlation in the He ground state. Similar conclusion have been drawn more recently from experiments on He single photon double ionization.[23]

The above presented argumentation is supported by theory.[21,22] In Figure 10 the angular distribution of the emitted electron 2 is shown in comparison with a theoretical prediction[21] for capture from non-s^2 contributions. The agreement between experimental data and theory is rather good supporting the explanation given here[20–23] yielding evidence that the observed momentum pattern are due to the momentum correlations of the non-s^2 contributions in the He ground state wave function. For pure s^2 contributions an isotropic angular distribution is predicted. It is surprising that the momentum correlation of such non-s^2 contributions can experimentally be separated and visualized by high-resolution momentum imaging.

It is to notice, that the kinetic energy difference of the recoiling He^{2+} nucleus between the different possible capture channels is rather small in the order of a few 10 meV. To measure such small energy differences this is experimentally a more difficult challenge than measuring the very small Lamb-shifts with high-resolution spectroscopic methods. The here explored initial momenta of electron 1 and 2 are 6.4 a.u. and about 4 a.u., corresponding to kinetic energies of about 560 and 220 eV, respectively. The sum of these kinetic energies is above the total binding energy of 79 eV of both He electrons in the ground state. By varying the projectile velocity the correlation of different non-s^2 contributions in the He ground state can be explored as function of their initial momenta.

According to theory[20] the electron momenta increase with increasing angular momentum thus electrons in the non-s^2 contributions have in average much higher velocities, i.e., momenta, than in the s^2 state. The non-s^2 contributions density peaks also at larger distances from the nucleus than the s^2 one.

3.3. Einstein's Double Slit Experiment: Investigated by Young-Type Interference Structures in Slow H_2^+ + He Collisions

In the famous Bohr–Einstein debates Albert Einstein pointed at an apparent problem in the quantum interpretation of the

**ADVANCED
SCIENCE NEWS**

www.advancedsciencenews.com

annalen
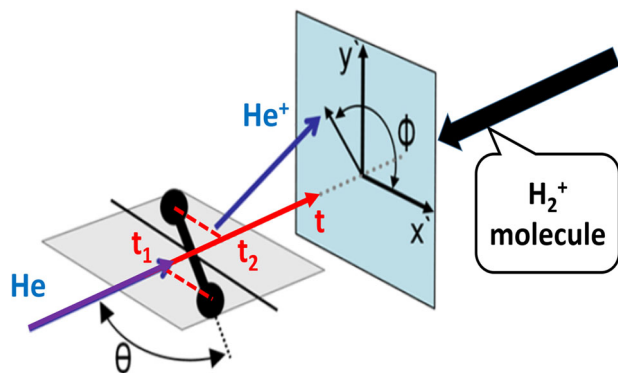der **physik**

www.ann-phys.org

Figure 11. Nuclear scattering plane defined by the internuclear axis of the H_2^+ ion and its velocity vector.[26] In inverse kinematics the He target atom collides with the H_2^+ molecular ion and transfers one electron to the H_2 molecule which breaks up into neutral H atoms. The two H atoms are detected angular resolved in forward direction. The He^+ ion momentum is detected with a C-REMI. The He^+ is scattered into the azimuthal angle Φ. The relative orientation of the molecule to the He impact direction is defined by the angle Θ. The time difference $t_2 - t_1$ can be determined from the measured angle Θ and the ion velocity. The thick black arrow shall indicate that in the laboratory system the H_2^+ ion is moving and the He target atom is at rest.

double slit experiment, e.g., like in case of electrons pathing through a double-slit system, "Einstein suggested that a control of the momentum transfer would permit a closer analysis of the phenomenon and, in particular, to decide through which of the two slits the electron had passed before arriving at the plate" (quotation from Bohr's account of the debate[25]).

Using C-REMI a realization of the Einstein Gedankenexperiment was recently performed, where the momentum exchange of the scattered projectile with the slit system could be measured.[26] The double slit was realized by using two nuclei of the H_2 molecule as coherent scattering centers representing the two slits. This was achieved for the collision system

$$10\,keV\ H_2^+ + He \rightarrow H_2^* + He^+ \rightarrow H + H + He^+ \tag{3}$$
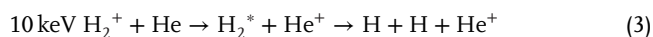
The momentum vectors of all reaction fragments in the final state were measured in coincidence. Thus, the orientation angle θ of the H_2^+ molecule with respect of the projectile momentum vector was determined for each event yielding the He^+ scattering distribution also in dependence of θ (**Figure 11**). Because of conservation of the total momentum the experiment allowed that for each single event even the impact position and impact time for the last arriving H atom on the detector could be predicted before its impact.

The question of this experiment was, does interference occur despite the fact that the momentum of the protons could be measured? Summing over all single-event measurements, the scattering distribution gave a positive answer to that question and "surprisingly" showed interference structures ("Young-type interference structures") in accordance with Bohr's interpretation (**Figure 12**).

The scattering at the left proton is accompanied by a momentum transfer to the left proton leading to a counterclockwise rotation of the molecule and the scattering at the right proton is accompanied by clockwise rotation, since both protons are
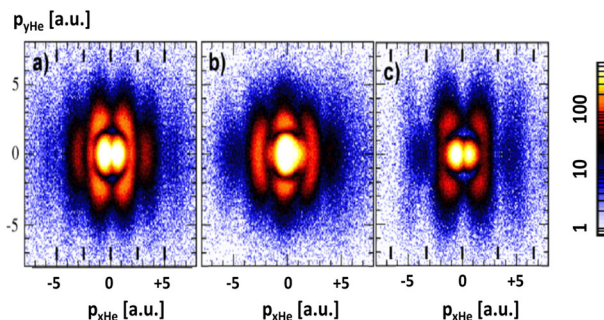

Figure 12. Two-slit interference pattern in the plane perpendicular to the projectile momentum vector for three different θ angles. a) Events for molecular orientation angles (with respect to the beam direction) from 80° to 90° and KER* values 1 to 2 eV. This KER corresponds to inter-nuclear distance values R from 2.3 to 2.9 a.u. b) Events for molecular orientation angles from 50° to 60° and KER 3 to 4 eV. This KER corresponds to R values from 2.3 to 2.9 a.u. c) Events for molecular orientation angles from 80° to 90° and KER 3 to 4 eV. This KER corresponds to R values from 1.7 to 2.0 a.u.[26]
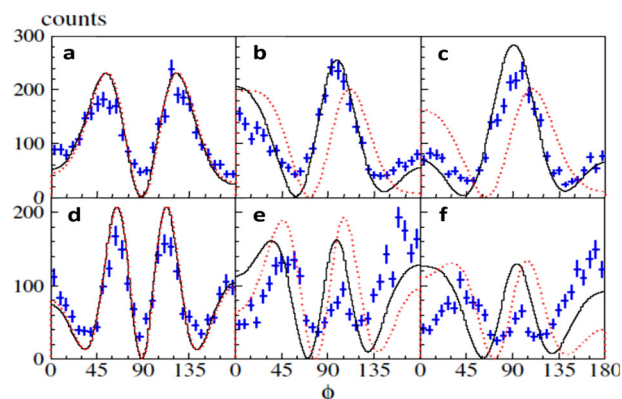

Figure 13. Relative cross-sections as function of the angle φ in comparison with model calculations (red dashed lines) and full theory (solid lines).[26] The left column represents collisions where θ is from 85° to 90°, the middle column where θ is from 55° to 60° and the right column where θ is from 45° to 50°. The rows show data for different transverse momenta and slightly different KER values.

bonded by the Coulomb force to one molecular unit. Thus the experimenter does not know on which proton the projectile was scattered. Quantum mechanically the two possible pathways of scattering of the He^{1+} at the left and right proton interfere. Thus the occurrence of the interference shows that the molecule is left in a coherent superposition of simultaneously rotating clock- and counterclockwise. The finding is at odds with our classical intuition as most of the puzzling quantum phenomena. It shows that the correct interpretation of the double slit experiment is not only that the particle "takes both pathways" but even more counterintuitively also transfers the full momentum sign onto the two slits. Figure 12 also shows that the interference pattern vary with θ and even with the KER value (electronic excitation), too. Schmidt et al.[26] presented a model calculation (red dotted line in **Figure 13**) for the superposition of the scattering amplitudes at the two H atoms. Depending on the angle θ the two amplitudes are shifted in phase ß. The phase difference between both amplitudes due to the molecular orientation θ is proportional to the

**ADVANCED
SCIENCE NEWS**

www.advancedsciencenews.com
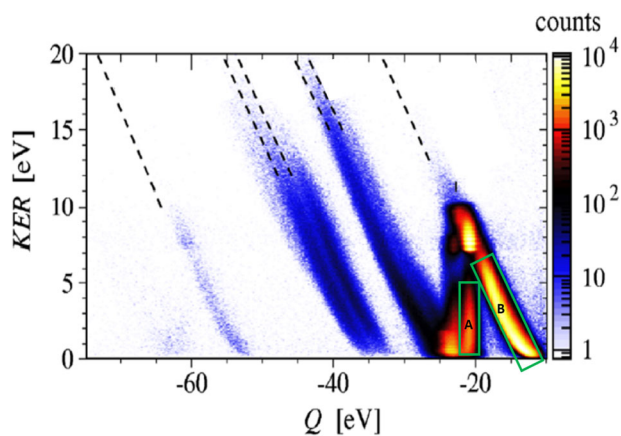
annalen
der **physik**

www.ann-phys.org

Figure 14. Final state KER-Q-value correlation diagram of the different electronic excitation channels. The lines mark different exited states. The channels A and B are discussed in ref. [26].

measurable delay time ($\Delta t = t_2 - t_1$ in Figure 11). In a multiparticle coincidence measurement one can calculate it directly from the measured angle θ and from the ion velocity v. The differential scattering cross-sections can be expressed as $d\sigma/d\varphi \approx \cos^2(\beta/2)$ where the phase shift ß is ß $= \pi + R \bullet \Delta p_{He}/\bar{h} + \Delta E \bullet \Delta t/\bar{h}$. The phase jump π accounts for the inversion of the molecular symmetry in the electronic transition and the second term for the change of the He momentum Δp_{He} due to the scattering, which leads to a change of the de Broglie wave length of the scattered He and for the term $\Delta E \bullet \Delta t/\bar{h}$. It accounts for the correction of the so-called translation factor with $\Delta t = t_2 - t_1$ as time difference of the interaction of the He projectile with the two H atoms.

In Figure 13, the measured interference pattern are compared with these model calculations (red dotted lines) and the full theory (black solid lines).[26] The data are presented for a given polar scattering angle (i.e., impact parameter) as function of the azimuthal angle Φ. In the left part (a) of Figure 12 the data are shown for $\theta = 90°$ and $\Delta t = 0$. In the middle part (b) $\theta = 60°$ and the right part (c) data are shown for $\theta = 45°$ where the influence of the delay Δt on the scattering as well as electronic excitation becomes strongly visible. The electronic excitation processes as function of the delay Δt does vary. The data of Schmidt et al.[26] prove in a convincing manner that the phase shifts can be measured with about 3° resolution. From these phase shifts time delays in the low attosecond range can be deduced.

Since the overall momentum resolution is so excellent, the different channels of electronic excitation in these scattering processes can be resolved event by event, too. Thus one can identify different electronic promotion channels during the collision. From **Figure 14** one can deduce that for each event the different electron promotion channels (different molecular orbitals) are fully separated by their KER and Q-value. The different electronic promotion pathways are marked by the letters A and B.

3.4. Visualization of Directional Quantization of Quasi-Molecular Orbitals in Slow Ion–Atom Collisions

During the very short duration of an ion–atom collision (typically attosecond range) so-called quasi-molecular orbitals are formed

across, which bound electrons can be promoted into continuum states. These orbitals should show directional quantization with respect to the nuclear scattering plane. How the experimenter can visualize this directional quantization of such short living angular momentum states?

Averaging over all orientations of the nuclear scattering plane, the electron emission pattern cannot show any sign of directional quantization. If the momentum vector of the emitted electron is measured with respect to the nuclear scattering plane by an electron–recoil ion–projectile coincidence the angular emission pattern should directly reflect this directional quantization. The existence of such a directional quantization also in electric field was already indirectly seen in the Stark effect and in impressive detail directly observed in electron spectroscopy of Auger type decays of electronic quasi-molecular states.[27] Later experiments using C-REMI by Dörner et al. and Abdallah et al.[28] and recently by Schmidt et al.[29] showed such directional quantization also for direct transitions to the continuum in slow 10 keV He^{2+} + He > He^+ + He^{2+} + e transfer ionization processes. The comparison between experiment and theory shows perfect agreement and proves that also in very shortly existing quantum states directional quantization occurs (see **Figure 15**). It proves that angular momenta have a strong influence on the ionization dynamics in such ion–atom collisions.

3.5. Direct Observation of the H_2^+ Vibrational Wave Function in Momentum Space

Schmidt et al.[30] succeeded to image the nuclear H_2^+ vibrational wave function in momentum space using C-REMI technique. They dissociated the H_2^+ molecule by electron attachment in 2.5 keV H_2^+–He collisions. Due to the achieved excellent momentum (and thus kinetic energy resolution) they could resolve the single vibrational states. The measured final fragment momenta are due to the motion in the initial vibrational state of the nuclei and due to the acceleration gained in the Coulomb field, when the molecular ion explodes.

From the measured momenta the kinetic energy release KER and the Q-value (internal excitation energy of the final state) were determined event by event. In **Figure 16** the raw data are shown.

They obtained a momentum resolution close to the quantum limit.[30] Such a resolution is not achievable with traditional methods like X-ray or electron scattering. To transform these data from the momentum space into the spatial internuclear coordinate R one has to make assumptions on the motion of the nuclei in their initial state. Schmidt et al. have performed transformations based on different assumptions: the most simple one is to take frozen nuclei.

In case of frozen nuclei the nuclei are at rest at the instant of the excitation process. The measured momenta are only due to the acceleration of the nuclei by the repulsive Coulomb potential. Thus from the measured KER value and the theoretically obtained quasi-molecular correlation diagram (two-center internuclear distance R versus potential energy, see **Figure 17**) the spatial density distribution (e.g., for the excited state $v = 3$) as function of R was deduced and plotted in **Figure 18** (green dots). Assuming initially moving nuclei one obtains a density plot which is shown by the red dots. Both differ strongly and are not in agreement with
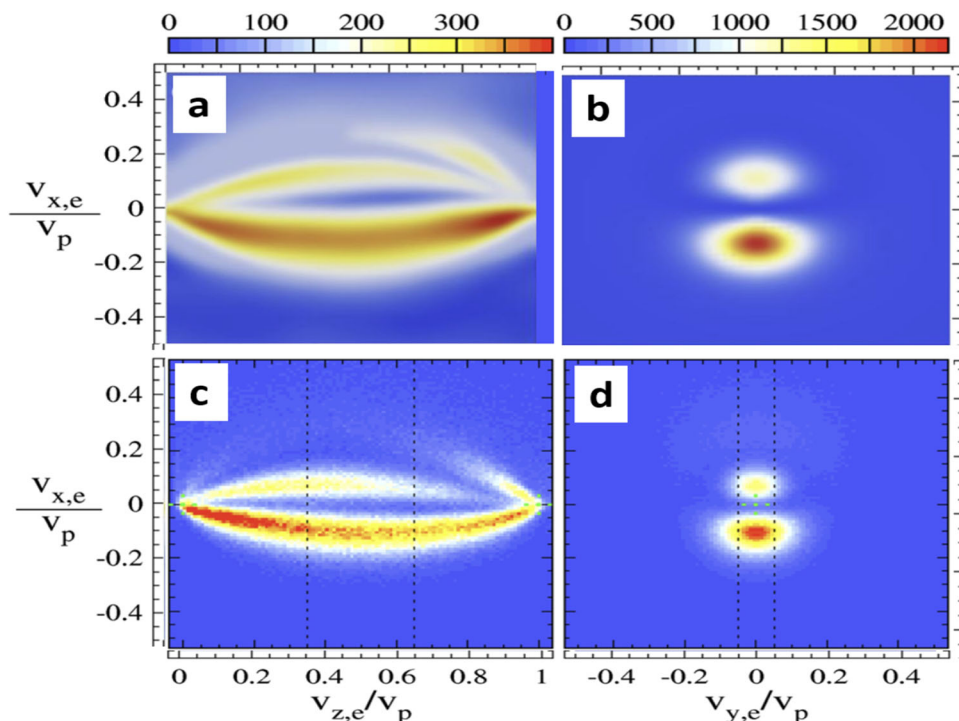
Figure 15. Electron momentum plots in 10 keV He^{2+} + He → He^+ + He^{2+} + e transfer ionization processes.[29] The abscissa and the ordinate are in units of the projectile velocity v_p, i.e., the electron momenta. Panels a,b) Theoretical predictions and c,d) experimental data. Panels (a) and (c) depict the projections on the nuclear scattering plane and (b) and (d) perpendicular to it.
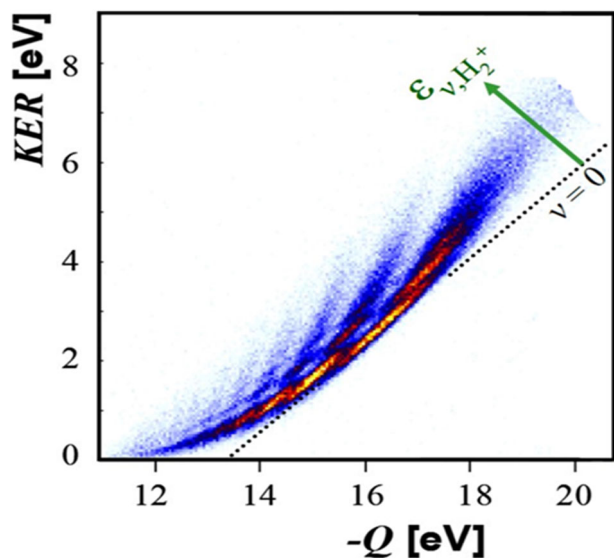

Figure 16. Density plot of the measured momentum distribution of the dissociated molecule as function of KER value and Q-value.[30b]

Figure 17. Scheme of reflection approximation in H_2^+ − He => 2H + He^+ collisions. The electron transfer occurs at $R = 2$ a.u.[30b]

the full quantum mechanical prediction (solid line in Figure 18). If one assumes that about half the kinetic energy in the initial state contributes to the finally measured KER value one obtains reasonably good agreement with the solid line. In **Figure 19** the measured density plots are shown of the lower H_2^+-vibrational states as function of KER and Q-value.
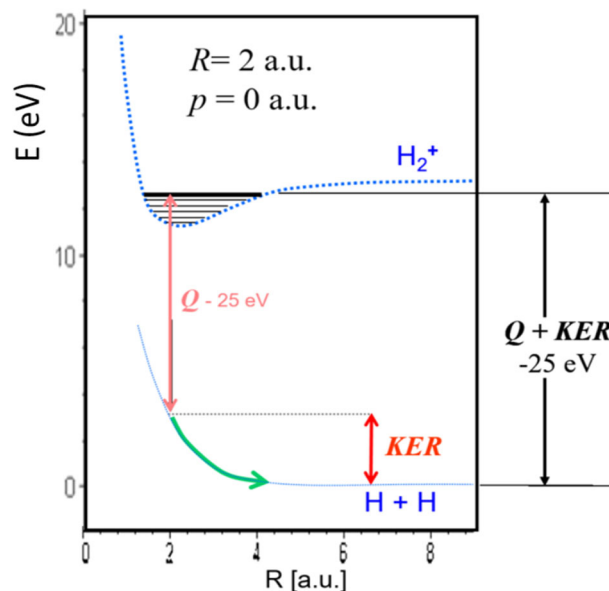
3.6. Experimental Separation of He-Ionization in Photo- and Compton Effect

Since the early nineties C-REMI was also successfully applied to explore photon-ionization processes. At this time an unsolved
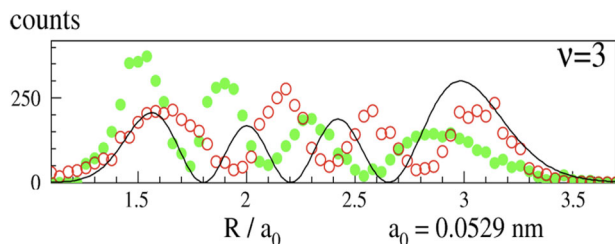
**ADVANCED
SCIENCE NEWS**

www.advancedsciencenews.com

*annalen
der* **physik**

www.ann-phys.org

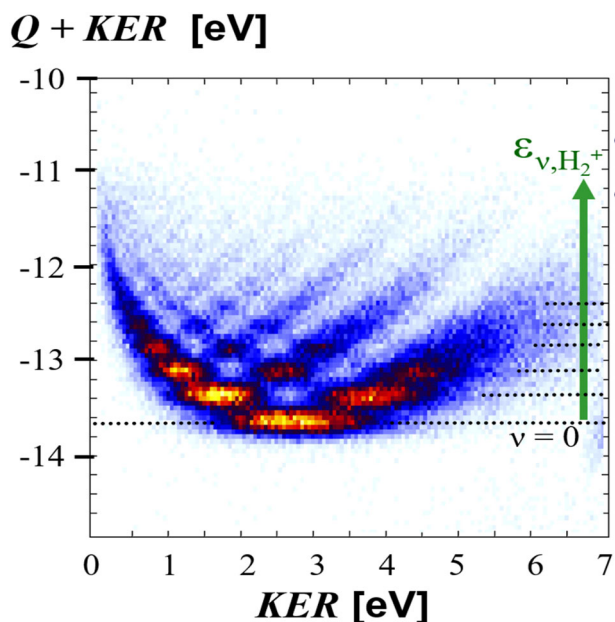**Figure 18.** Spatial density of the vibrational state $v = 3$ (see text).[30]

Figure 19. Density plot of H_2^+-vibrational states as function of KER and Q-value.[30b]

fundamental problem in photon physics was the measurement of the ratio of the total ionization cross-sections of helium in case of photon-ionization compared to ionization caused by the Compton effect. The traditional methods of ion counting could not distinguish by which mechanism the atom was ionized. Both processes, however, differ in their recoil ion kinematics. In case of the photoeffect the momentum p_e of the ejected electron is fully balanced by the recoil ion momentum with $p_{recoil} = -p_e$ (see **Figure 20**, left side). In case of the Compton effect the recoil ion acts only as a spectator and its final momentum remains close to zero (see Figure 20, right side). Using the C-REMI approach, these different recoil ion momentum distributions could quite easily be measured and be separated.[31]

In Figure 20 (left side) the outer ring (dipole distribution) corresponds to electrons were the second electron remains in the He-ground state. The inner rings represent processes, where the second electron is excited into higher orbitals. One can see that when the other electron is exited these distributions are not anymore dipole-like distributions due to electron correlations. The ratios of the total cross-sections were measured at different photon energies (see **Figure 21**).[32] They were in good agreement with many-body perturbation theory MBPT.[33]

3.7. Multiphoton Processes: Experimental Verification of the Rescattering Mechanism

The total double ionization rate of He in strong laser fields at not to high intensities showed an enhancement of many orders of magnitude over the values expected from two sequential single-ionization processes (see blue solid line in **Figure 22**, left part[34]). Corkum and Kulander et al. proposed as explanation a nonsequential process, the so-called rescattering mechanism[35] (see Figure 22, right part). According to their hypothesis the electrons emitted in the laser field are oscillating in the strong field and are then rescattered at their parent atom and knock out the other electron.

When in the nineties this hypothesis was proposed it could experimentally not be proven and verified, since the strong-field community did not have the proper detection device. To visualize the dynamics of this rescattering process one had to measure in coincidence the momenta with high resolution of two or more ejected low-energetic electrons (and if possible of the recoil ion, too).

A few years later using the C-REMI method the dynamics of such an ionization process was investigated. The Heidelberg group of Ullrich and Moshammer, who supplied a C-REMI, joined the laser group of Sandner and Rottke in Berlin[36] and, parallel in time the Frankfurt group of Dörner and Weber, who supplied the C-REMI, joined the group of Giessen in Marburg who provided the laser.[37] Presented here, in **Figure 23**, are the data of the experiment performed in Marburg.

For 220 fs long laser pulses of 800 nm wave length at intensities of 3.75 and 15×10^{14} W cm^{-2} the Ar^{2+} and He^{2+} ionization process was investigated by performing an electron-recoil coincidence. Thus the momentum vectors for both emitted electrons were determined in each event and the complete momentum exchange was measured. In Figure 23 the momentum vector correlations of the two electrons are shown for two different laser intensities. For the more intense laser pulse (right part) the electron vectors show a distribution similar to the one expected for two sequential single ionization processes. For the lower laser intensity (left part) the momentum pattern changes completely. It shows that the two electrons are preferentially emitted to the same hemisphere (contribution in the first and third quadrant of Figure 23). This correlated electron emission proves that the electrons are born close in time and experience the same vector potential.

The observed structures in the momentum distribution plots are in full agreement with the predictions of the rescattering model. The surprising result was: the He^{1+} recoil momenta are strongly directed parallel to the laser electric field with much smaller momenta in the transverse direction—even much less than in case of single photon ionization. The He^{2+} recoil ion momenta are in transverse direction of the laser field similar to the He^{1+} momenta, but parallel to the field 5 to 10 times larger (Figure 23, bottom part). In addition, they show two maxima separated by a minimum at zero momentum. In case of single photon ionization, the recoil ion momentum distribution reflects mainly the momentum distribution of the electron in its initial bound state, in case of double ionization by a single photon it reflects possible electron–electron correlations in the initial state. But the He^{2+} recoil momenta never exceed the

**ADVANCED
SCIENCE NEWS**
www.advancedsciencenews.com

annalen
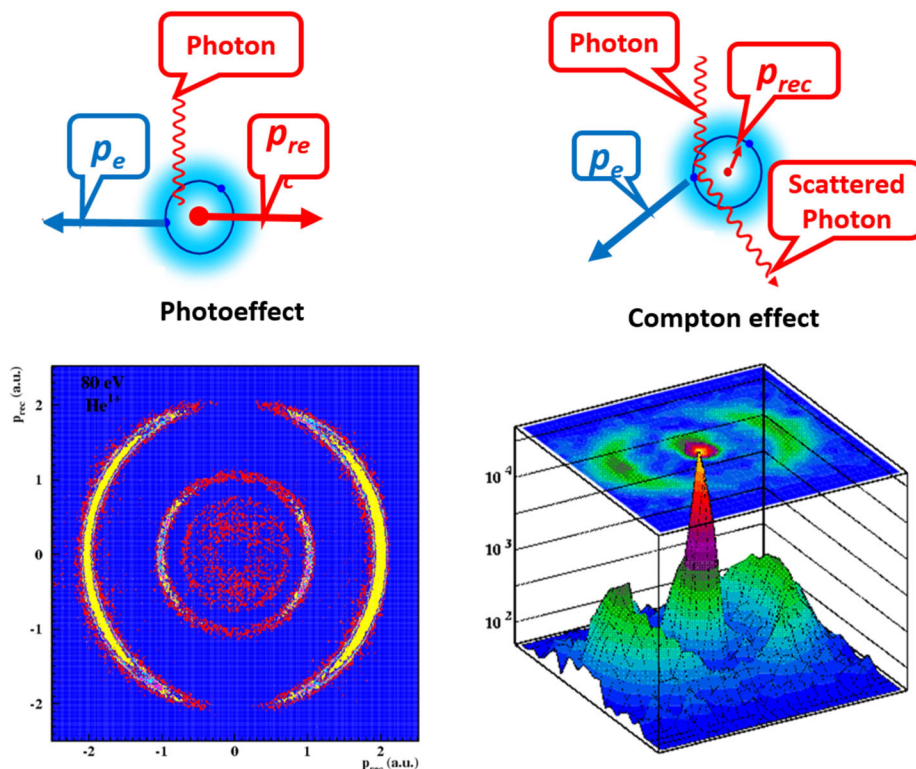der **physik**
www.ann-phys.org

Figure 20. Recoil ion momentum plots measured by C-REMI in case of He photon ionization by 80 eV linear polarized photons (left) and Compton process ionization by 8.8 keV linear polarized photons (right). The upper parts show the schemes of the momentum exchange.[31d]
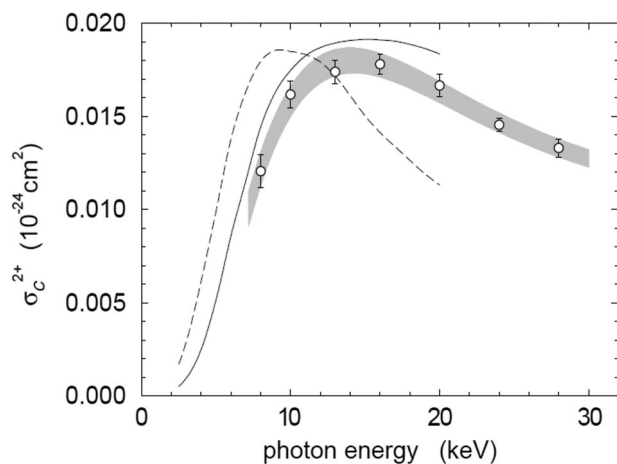

Figure 21. Compton ionization cross-section in helium (open circles). The shadow area and lines represent calculations of Bergstrom et al.[33]

Figure 22. Strong field single and double ionization cross-sections of helium.[34]

He^{1+} recoil momenta by more than a factor two. Thus, in case of laser induced double ionization only Corkum's rescattering mechanism can explain the observation of such large He^{2+} recoil ion momenta parallel to the laser field. In his model, the electron can gain in the laser field a high ponderomotive energy yielding finally a large recoil momentum. The work by Weber et al.[37] and Moshammer et al.[36] provided a clear experimental proof that the rescattering process does explain the dynamics of the double ionization in intense laser field. More work on strong
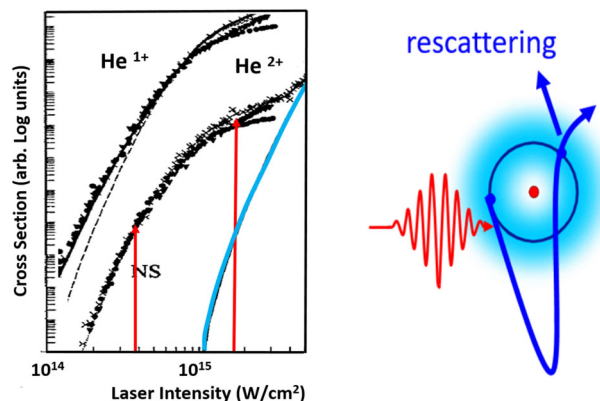
laser field ionization investigated by C-REMI can be found by consulting the work of Weckenbrock et al.[38]

3.8. Multivector Correlation Measurements in Molecular Fragmentation Processes: Search for Dynamical Symmetry Breaking and Observation of Aligned Very Short-Living Exotic States

C-REMI allows to study the detailed decay dynamics of a multiparticle fragmentation process of molecules. By measuring with high resolution the momentum vectors of all emitted electrons
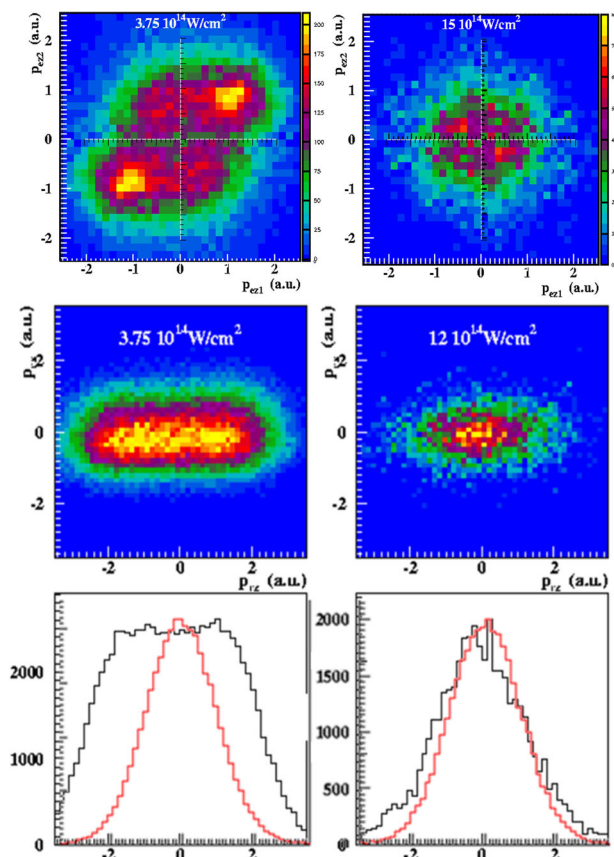
**ADVANCED
SCIENCE NEWS**

www.advancedsciencenews.com

annalen
der **physik**

www.ann-phys.org

Figure 23. Upper part: density plot of momentum of electron 1 versus momentum of electron 2 for the two different laser intensities for double ionization of Ar (see text) projected on the plane perpendicular to laser impact direction. Middle part: density plot of He^{2+} recoil momentum for two different laser intensities. Lower part: projection of the recoil momentum distribution on the z-axis. Black line: doubly charged ions, red line: singly charged ions.[37d]

Figure 24. Scheme of a fragmentation chain with intermediate steps 1 to 6.

and ionic fragments in the same event the entangled many-particle dynamics in the molecular system can be explored.

The fragmentation process is triggered by a single high-energetic photon which is absorbed by the molecule creating an inner-shell vacancy (e.g., in a K-shell of one atom in the molecule). Performing the experiment even for right- and left-handed circular polarized photons the experimenter knows the angular momentum orientation of the excited molecule. In the first decay step (see **Figure 24**) a photoelectron is emitted. An excited molecule remains. From the kinetic energy of the photoelectron the vacancy state can be determined. After a very short delay (attoseconds to a few femtoseconds) the excited molecule will decay step by step by emitting more Auger electrons finally ending in Coulomb explosion by repulsion of the positively charged nuclei. From the kinetic energies of the Auger electrons the sequence in time of the Auger-electron cascade can unambiguously be identified. Thus the experimenter knows the time sequence of the decay steps, however, the time delays between each emission step remain unknown. The measurement of the momentum vectors of the ionic fragments provide the orientation of the molecule at the moment of ionization in the
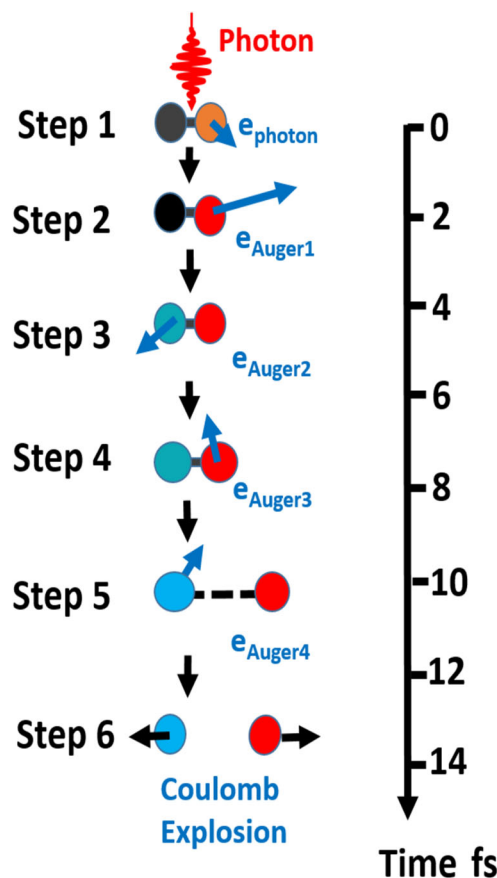
laboratory system. Thus the experimenter has performed a "complete" experiment of the dynamics of the fragmentation process. The experiment can even explore whether any dynamically induced symmetry breaking (in time or parity) may occur.

To search for such signs of dynamical entanglement and symmetry breaking the experimenter can investigate whether electrons emitted in step n have a "memory" of the earlier fragmentation steps. From the measured vectors L_γ and p_{fn} (L_γ is the angular momentum vector of the photon and p_{fn} the momentum vector of the nth emitted electron) the experimenter can define new dynamical coordinate systems based on vectors, e.g., like $L_\gamma \times p_{f1} = Z_{y1}$ and $p_{f1} \times p_{f2} = Z_{12}$. Plotting in the later steps emitted electron-emission probabilities with respect to these new coordinates[39] for right- and left-handed photon ionization the data may show asymmetries indicating symmetry breaking.

This experimental approach enables thus the investigation of fundamental dynamical processes in many-particle systems, like time or parity symmetry breaking. This vector equation

$$Z_{Ly1}(-t) = L_\gamma(-t) \times p_{e1}(-t) = (-) L_\gamma(+t) \times (-) p_{e1}(+t) = +Z_{Ly1}(t)$$

(4)

proves that in case of time inversion the vector $Z_{Ly1}(t)$ does not change its sign. If time symmetry is valid the in time mirrored

**ADVANCED
SCIENCE NEWS**

www.advancedsciencenews.com

*annalen
der* **physik**

www.ann-phys.org

Table 1. Vector products with respect to time and parity symmetries.[39]

Vector product	$T \rightarrow -t$	$R \rightarrow -r$
$Z = A_y \times p_{ephoto}$	$Z(t) = +Z(-t)$	$Z(r) = -Z(-r)$
$Z' = (A_y \times p_{ephoto}) \times p_{k\text{-Auger}}$	$Z(t) = +Z'(-t)$	$Z''(r) = -Z''(-r)$
$S = (A_y \times p_{ephoto}) \cdot n$	$S(t) = +S(-t)$	$S(r) = +S(-r)$

data should be identic. If time symmetry is broken then the distribution of the Auger electron of step 2 with respect to vector $Z_{Ly1}(+t)$ (p_{e1} is the momentum vector of the photoelectron) and to vector $Z_{Ly1}(-t)$ should be not symmetric. In **Table 1** some "dynamical" vector products are listed with respect of time and parity symmetries.

For 306 eV right- and left-handed photons on carbon monoxide CO the vector correlations between the 10 eV photoelectron, the K-shell Auger electron (carbon), and the singly charged ionic fragments were measured.[39] In **Figure 25** for right-handed (right part) and left-handed (left part) the angular distributions of the photoelectron emission are plotted. The molecular orientation is shown by the bar-bel, respectively. The data show the strong influence on the photon handedness. The red dashed line on the left side represents the distribution of the right side (right-handed photons) mirrored in time ($t => -t$). The small differences in the intensities under 130° and 300° are probably due to different contributions of linearly polarized photos and uncertainties in the photon polarization angle in the primary incoming photon beam.

Trinter et al.[39] analyzed their coincidence data with respect to possible dynamically induced symmetry breaking by plotting the K-Auger electron distributions (step 2) for different conditions (emission angles) on the momenta of the emitted photoelectrons for both left- and right-handed photons. However, these are preliminary measurements and originally not performed to search for symmetry breaking effects. Possible unknown errors cannot be excluded. The preliminary data are mentioned here to show that such fundamental aspects of possible symmetry breaking in quantum dynamics can be explored with the C-REMI approach in such kind of vector correlation measurements. In another experiment on N_2 innershell ionization Schöffler et al. clearly showed the entanglement between photoelectrons and Auger electrons.[40]

Furthermore such a vector-correlation measurement approach provides the possibility to study oriented extremely short living excited atomic and molecular ionic configurations, which can never be produced by any other preparation technique (e.g., like laser pump and probe technique).

As shown in Figure 24 in subsequent steps several Auger electrons can be emitted, thus the experimenter observes a cascade of excited states which are all dynamically entangled. Because of the excellent C-REMI momentum resolution an energy loss by photon emission might be even indirectly detectable too. The life time of these intermediate excited states (typically attoseconds up to a few femtoseconds), however, cannot be detected by C-REMI in a direct way but it might be possible to deduce from the measured KER values, which vary with time due to the Coulomb explosion, information on the delay times.
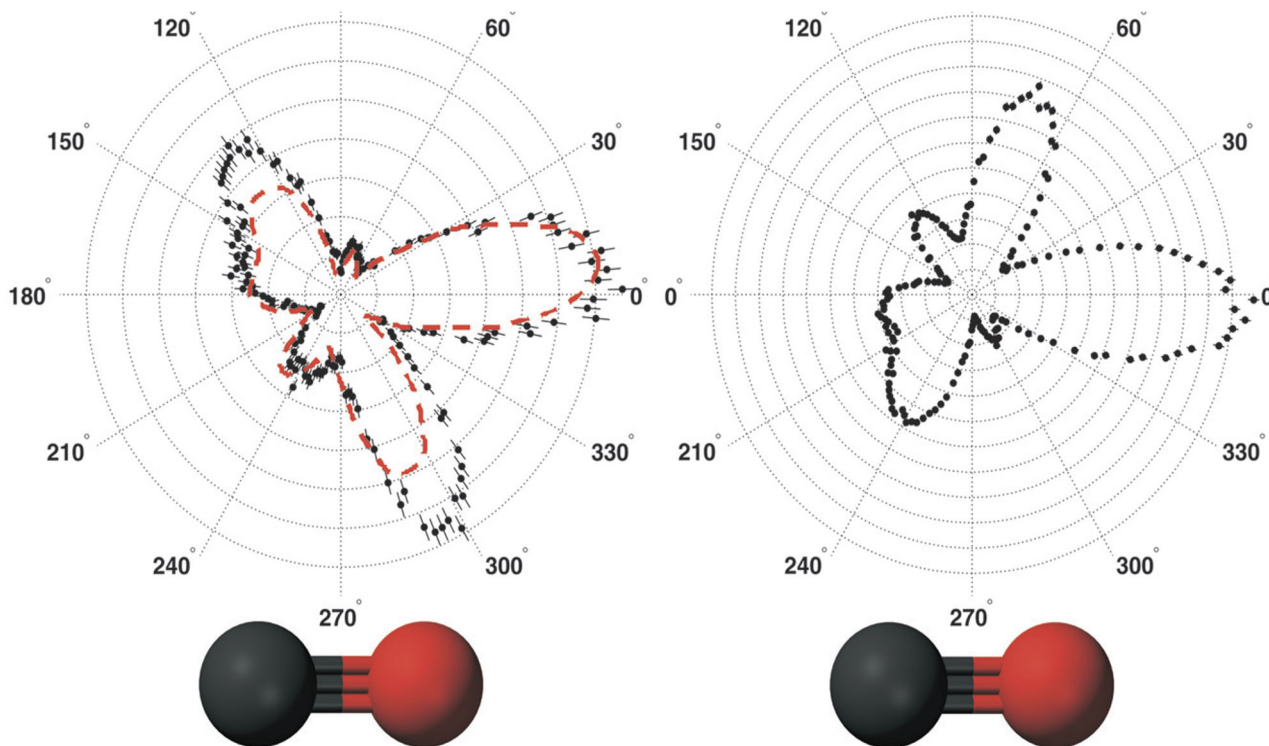

Figure 25. Polar plot of angular photoelectron distributions in the plane perpendicular to the propagation of the photon. Left: the red dashed line represents the distribution of the right side (right-handed photon) but mirrored in time. The molecular orientation is indicated by the bar-bell with carbon on the left. Only events with a KER value > 11 eV are selected, which ensures the axial recoil approximation.[39]

**ADVANCED
SCIENCE NEWS**

www.advancedsciencenews.com

*annalen
der* **physik**

www.ann-phys.org

This method would provide a kind of "One-Photon Pump and Multiple-Decay Probe" technique similar to the two-pulse laser pump and probe technique.

3.9. Single Photon-Induced Interatomic Coulombic Decay

More than twenty years ago Cederbaum et al.[41] discovered theoretically that electronically excited states in weakly bound molecules or in loosely bound matter can decay by exchange of virtual photons. The excitation energy can be transferred by means of a virtual photon between the excited atom and its neighboring atom. This decay channel was named "interatomic Coulombic decay" (ICD). First experimental evidence for the existence of ICD was reported by observation of slow electrons emitted in large photon excited Ne clusters by Hergenhahn and co-workers.[42] This process can occur already in very weekly bound molecules, for example, the Ne dimer, which is a prototype system for ICD. It is bound by van der Waals forces with a binding energy of 2 meV at an internuclear distance of 3.4 Å.

To yield a unique fingerprint of this ICD process one has to measure the entangled dynamics of this process by detecting the momenta of all fragments in the final state in coincidence. The kinetic energy of these fragments is rather low in the few eV range.

Jahnke et al.[43] have performed at BESSY II in Berlin a corresponding multifragment coincidence experiment using the C-REMI approach. The photon energy was chosen such that only a 2s electron in one Ne atom could be ejected. Thus a subsequent Auger transition in the same ionized atom was energetically not possible. According to the ICD mechanism the excitation energy is then transferred to the other atom of the dimer causing the ionization of its outer shell. The energy released in the process is shared by the ICD electron and fragmenting ions. The ICD in Ne dimers can be identified by coincident detection of two Ne^{1+} fragments and the low-energy ICD electron. Therefore, the total sum of the kinetic energies is fixed and can be used for an unambiguous identification of the ICD process.

The scheme of the ICD process is shown in **Figure 26**. The quantitative values of the shared energies are plotted in a 2D plot, KER energy versus electron energy in **Figure 27**. The characteristic ICD signature is the existence of the diagonal line in depicting the constant energy sum. From the Coulomb explosion kinematics and the measured KER value the experimenter can deduce the time scale of the ICD process with the help of the molecular correlation diagram.

In 2013 Trinter et al.[44] have investigated the ICD process in van der Waals-bound HeNe molecules. Najjari et al.[45] predicted that in such molecules one of the atoms can act as a very efficient antenna to absorb photons. In case of HeNe, the ionization cross-section is strongly enhanced if the photons can first interact with the He atom. It absorbs the photon and in an ICD-process the energy is transferred to the neighboring Ne atom which then emits an electron. In **Figure 28** (upper part) the different steps of this process are shown.

The measurement was performed with a C-REMI system detecting the emitted electron and ion in coincidence. Trinter et al. have experimentally verified that a single atom can act as a highly efficient antenna to absorb energy from a photon field and transfer the energy to a neighboring receiver atom within a few hun-
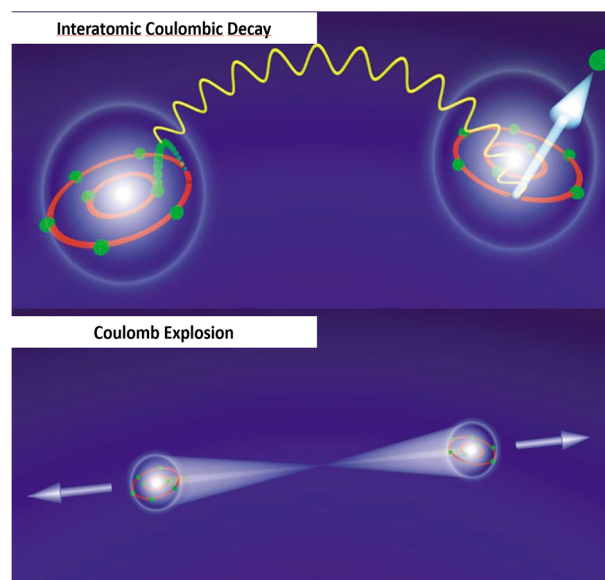

Figure 26. Scheme of the ICD process. Upper part: virtual photon transfer from the ionized atom to its neutral partner atom yielding the emission of a 2p electron from the partner atom. Lower part: Coulomb explosion of the doubly charged dimer.[43]
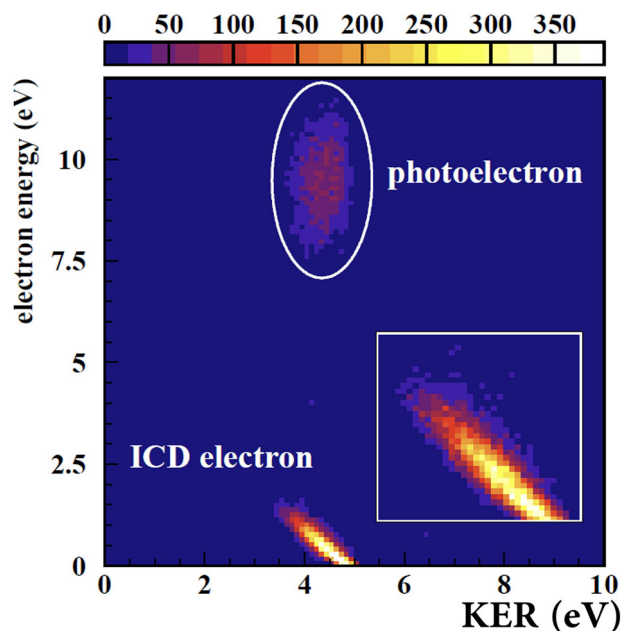

Figure 27. Kinetic energy release KER of the Ne ions versus the energy of photoelectron and ICD electron.[43]

dreds of femtoseconds. The resolved vibrational states of the resonance provided a benchmark for future calculations of the underlying energy transfer mechanism of ICD. More recent work on the ICD process is presented in ref. [45–50].

3.10. Laser P&P Measurements

To explore the nuclear dynamics in atomic and molecular reactions induced and manipulated by two strong subsequent
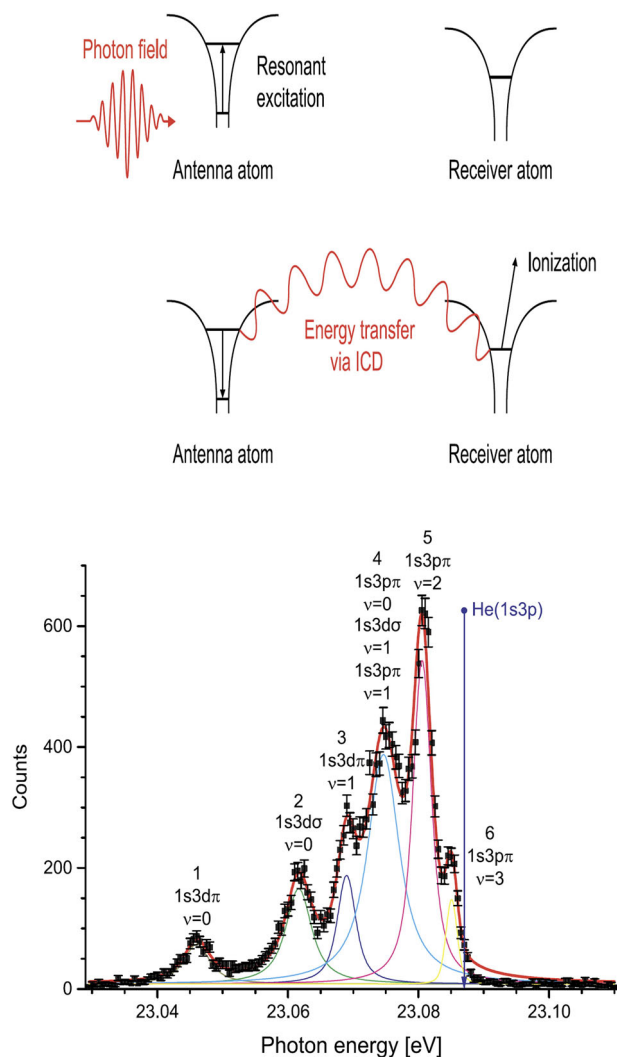
2100134 (16 of 25)

Figure 28. Upper part: scheme of absorption and decay steps. The photon coming from left is absorbed by the He atom, which is resonantly excited into the 1s3p state. Before it can decay by photon emission the excitation energy is transferred via resonant ICD to the neutral Ne atom, leading to its ionization. Lower part: the photon energy was scanned over the range of the He resonance below the actual ionization threshold. The vibrational states of the molecule can be nicely resolved.[44,45]

Figure 29. Scheme of the P&P experiment and the relevant potential curves of D_2 and D_2^+. The molecule D_2 is excited and ionized at $R \approx 1.4$ a.u. (0.7 Å) by the pump pulse from the ground state to the $1s\sigma_g$ state of D_2^+. The probe pulse ionizes the D_2^+ ion at $R*$ thus Coulomb explosion starts.

femtosecond laser pulses the experimenter has to detect emitted fragments (ions and electrons), which have typically very low kinetic energies. To demonstrate the power of the combined P&P and C-REMI approach two experiments are presented here: the one by Ergler et al.[51] and the other one for the experiment by Kunitski et al.[52]

Ergler et al. report on high-resolution real time imaging of D_2^+ nuclear wave packets. Their fast clock uses the Coulomb explosion dynamics. They visualize for the first time the spatiotemporal structure of the vibrational as well as the rotational wave function density up to the time period of 3000 fs. In **Figure 29** the scheme of the applied P&P approach is shown. The first laser pulse excites and ionizes the D_2 molecule from its ground state to the 1s-sigma state (the internuclear distance R remains unchanged
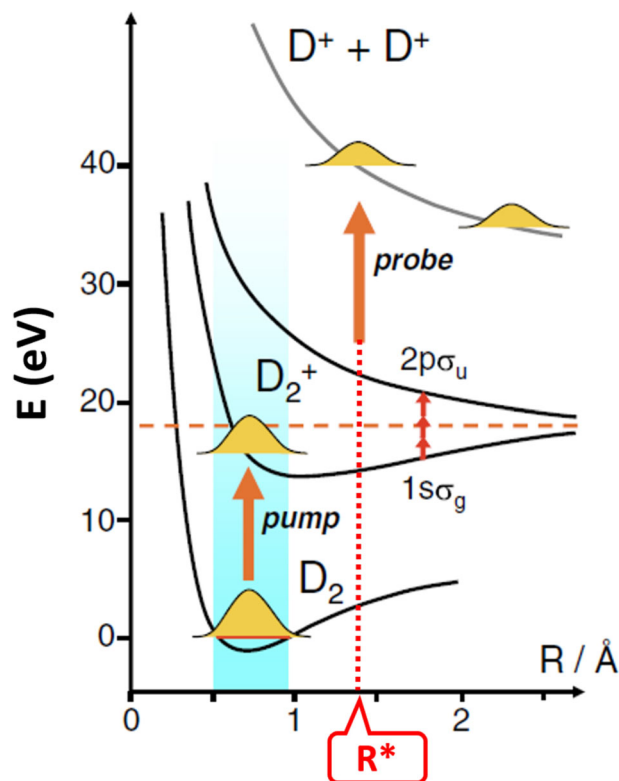
during the ionization process). After some delay the second more intense laser pulse creates complete ionization and thus provides a snapshot at distance $R*$ of the exploding molecule $D_2^+ => D^+ + D^+$. At this moment Coulomb explosion starts and provides a precise kinematical clock by transferring potential energy into kinetic energy of the fragments. The kinetic energies of the D^+ fragments can directly be determined from their measured momenta. In **Figure 30** the density plot of kinetic energies is presented as function of the delay time between both laser pulses. Three contributions[51] can be distinguished: a) a broadband centered at about 4 eV resulting from excited D_2^+ molecules, where Coulomb explosion did start with the second laser pulse (region 1), b) region 2, where the Coulomb explosion started already with the first pump pulse, and c) region 3, where the Coulomb explosion starts at large internuclear distances and the energy provided by absorbing photons is carried away by the emitted electrons.

For short delays (<100 fs) well resolved wave structures are present separated by about 24 fs descending in energy and corresponding to increasing internuclear distance. The oscillatory behavior reflects the motion of the vibrational wave packet launched by the first pulse on the 1s-sigma potential curve of D_2^+. Such a wave packet slowly disperses due to the slightly differing vibrational frequencies of the several vibrational states populated. However, after some time these different components of the wave packet come back into phase, resulting in the vibrational revival seen around 500 fs. With increasing delay the structure smears
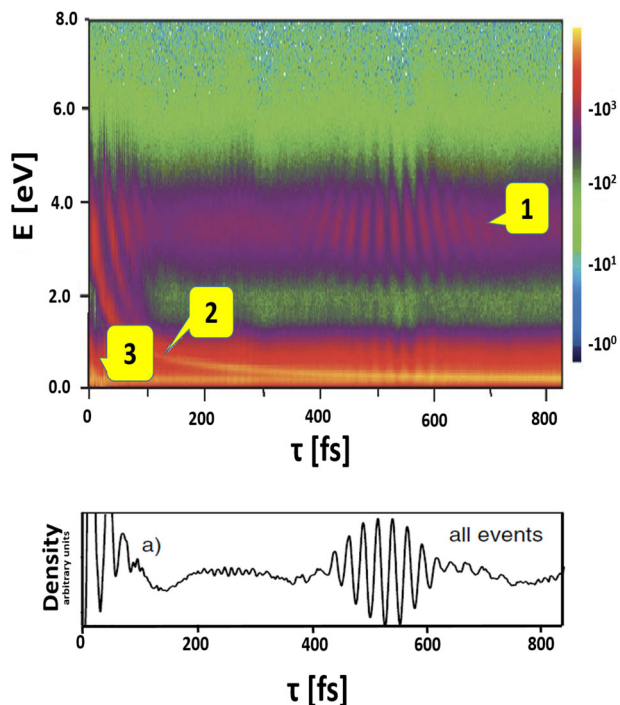
**ADVANCED
SCIENCE NEWS**

www.advancedsciencenews.com

annalen
der **physik**

www.ann-phys.org

Figure 30. Upper part: density plot of kinetic energies as function of the delay time τ between both laser pulses. The labeling 1–3 is explained in the text. Lower part: total wave packet densities as function of delay time summed over all angles.[51]

explosion starts. The probe pulse delivers thus a snapshot of the internuclear wave packet at this moment. The outward moving wave packet interferes with the long range tail of the bound part of the wave function. This interference makes it possible to visualize not only the density of the wave packet but also its wave function including the phase.

The influence of the laser field on the dimer can be seen in the alignment change of the molecular axis with respect to the direction of laser polarization. Θ is the angle between both directions. In **Figure 31**, left part, the density plot (colors) of the aligned wave packet is shown as function of the alignment angle $\cos(\Theta)^2$ and the delay time between pump and probe pulses. The calculated internuclear distance in Angström (1 Å ≈ 2 a.u.) is also shown. The C-REMI measurement visualizes alignment effects of the dimer in the laser field. This alignment changes with delay time, i.e., with internuclear distance. At about 1 ps a small alignment effect along the direction of polarization is visible, at ≈40 ps the inner part of the wave function appears isotropic in angle, whereas it displays again alignment. From these data information on the dimer wave function and thus on the potentials as well as on the dynamics inside the manipulated dimer at large distances can be deduced.

3.11. Structure of the He-Trimer Efimov State

As pointed out in Section 3.9 van der Waal forces can create bonding at huge internuclear distance. Efimov[54] predicted in the late 1960s of the last century a universal three-body state which does exist even when any two-body binding vanishes. These very exotic quantum objects are named "Efimov states." They can exist for any short range potential as, e.g., nuclear interaction or van der Waals interaction. For the van der Waals case the binding energy of the molecules is only a few hundred neV. Thus they can exist only at very low temperatures. It is extremely tricky to produce and separate them. It is even more tricky to explore their wave function and molecular structure.

Kunitski et al.[55] succeeded in 2015 to produce and identify He trimers in an Efimov state and even measure the vibrational wave function of the ^{4}He Efimov-trimer. They also employed the matter-wave diffraction technique of Schöllkopf and Toennies[56] to prepare the trimer target state. Then they multiply-ionized the trimers with a short, high intense laser pulse. This sudden ionization induced a Coulomb explosion of the trimer. Using the C-REMI approach, the momenta and thus the orientation of all ionic fragments were measured in coincidence. Based on theoretical trimer potential curves the momenta, respectively, the KER values, could be converted into internuclear distances. The obtained spatial structure of the measured excited state is shown in **Figure 32** (middle part), right and left parts represent theoretical predictions for the ground and excited states. The agreement between experiment and theory is very good. The Efimov trimer consists in principle of a He dimer with the third He atom orbiting at very large distances (>100 a.u.). This experiment has proven that C-REMI is able to clearly identify even very rare events in the presence of other hugely dominating processes or background, due to the coincident detection of all fragments with the precise measurement of momenta.
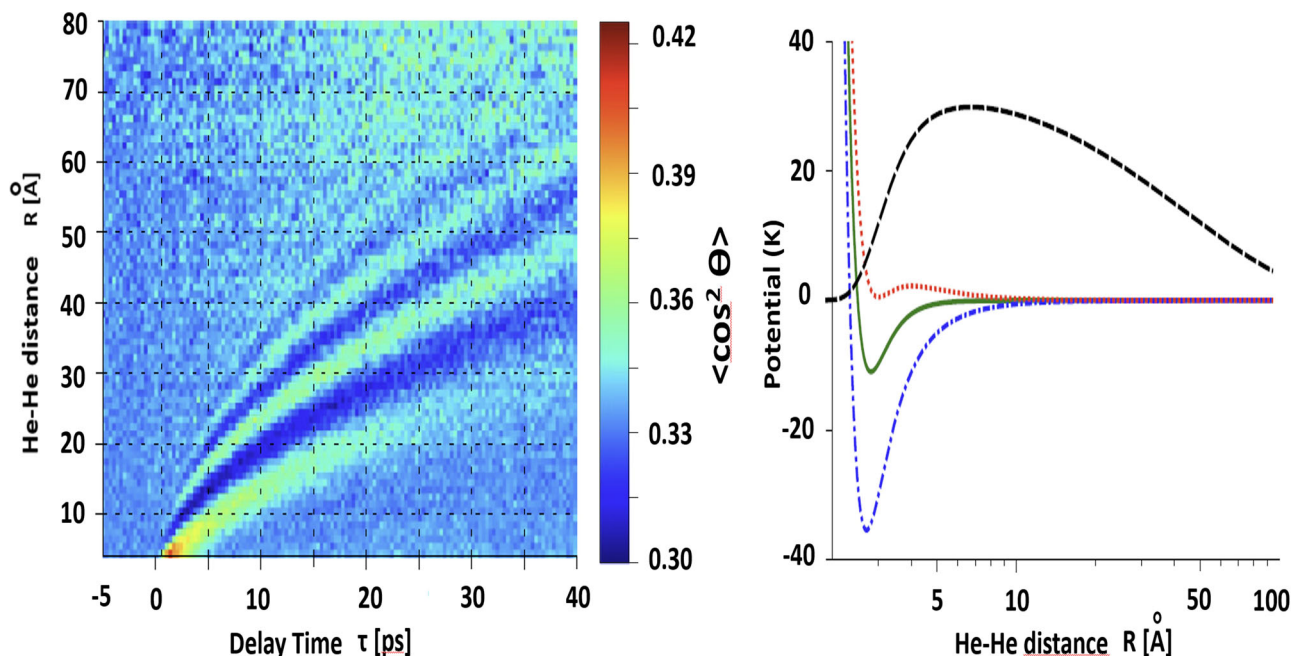
out, but surprisingly it is refocused after about 500 fs. Such a revival of the wave packet motion is discussed by Robinet.[53] The data in Figure 30 show also signatures of rotational motion[51] even in the low fs range. The data of Ergler et al. demonstrate clearly the excellent resolution power of C-REMI to explore the secrets of such ultrafast dynamical fragmentation processes.

Long range van der Waal forces remain since their discovery in the nineteenth century still a hot topic of research in physics and chemistry. Of particular interest are very weakly bound rare gas dimers or trimers since they show bonding even in more than several a.u. up to even a few 100 a.u. distance. It is experimentally extremely difficult to measure directly their molecular wave function and bonding dynamics at such large distances, because they exist only under special gas target conditions as very rare contributions. Thus one needs an experimental approach with high detection efficiency and excellent momentum (kinetic energy) resolution for charged rare gas ions of nearly zero kinetic energy. C-REMI provides all these required capabilities.

Kunitski et al.[52] have very recently successfully performed such investigations. Using two-pulse laser P&P technique they could manipulate such molecules and visualized by using C-REMI the dynamical behavior of such weakly bound atoms in the dimer. The first laser pulse tunes the interaction between the two He atoms in the dimer by transferring angular momentum to the molecule evoking an initially confined dissociative wave packet. This wave packet propagates to larger internuclear distances (several a.u.). After a delay in the picosecond range the second very intense laser pulse ionizes both atoms and Coulomb

Figure 31. Left side: density plot (colors) of the aligned wave packet as function of the alignment angle $\cos(\Theta)^2$ and the delay time between pump and probe pulses. Right side: interatomic potential of the He_2 dimer. Green solid line: native potential; Blue dashed-dotted line: laser field induced potential along the electric field direction. Red dotted line: laser field induced potential perpendicular to the electric field direction. The black dashed line presents the square of the wave function (arbitrary units) corresponding to the native potential.[52]
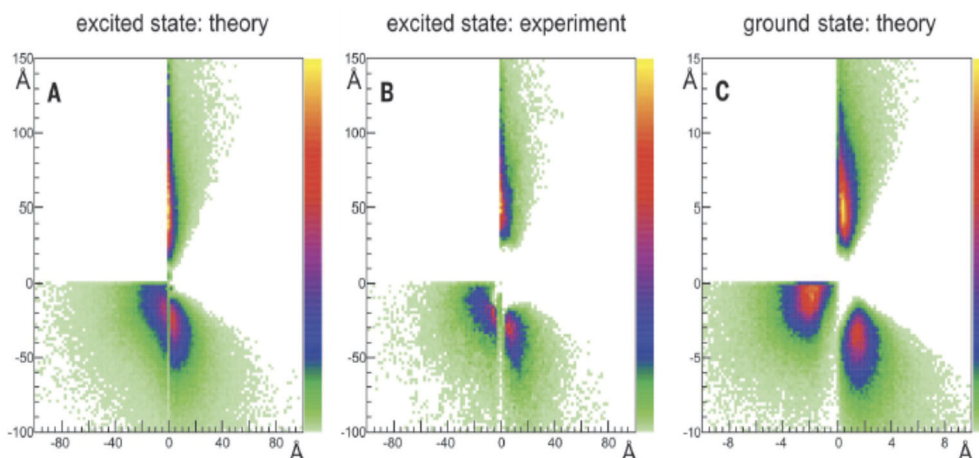

Figure 32. Structure of the He trimer.[55] A) The structure predicted by theory and B) the measured one for the excited Efimov state.[54] C) For comparison, the ground state structure as predicted by theory. Notice the factor of 10 difference in the size.

3.12. Imaging of Structural Chirality

Many pharmaceutical drugs have a chiral structure, they come in two enantiomers. The purity of drugs is a crucial condition for their application. Molecules of one handedness are beneficial for health and those of opposite handedness can be noxious. Even a very small impurity of the wrong enantiomer can be very dangerous. Thus it would be of great help if one can recognize for each molecule whether it has the proper handedness. A C-REMI can analyze molecules in the gas phase (and in the future eventually also drugs) and determine with ≈100% certainty

which handedness each molecule has. Pitzer et al.[57,58] and Fehre et al.[59] investigated by using a C-REMI the single-photon (710 eV) and strong-field induced complete fragmentation process of the chiral molecule CHBrClF. They were able to detect up to five ionic fragments in coincidence.[57,58] Even though the molecules are randomly oriented in the gas phase, as pointed out before, the coincident detection of momentum vectors of the ionic fragments allows for a determination of their orientation on a single molecule basis. Moreover, when investigating larger molecules, even the molecular structure can be reconstructed from the momentum measurement. As an example, the
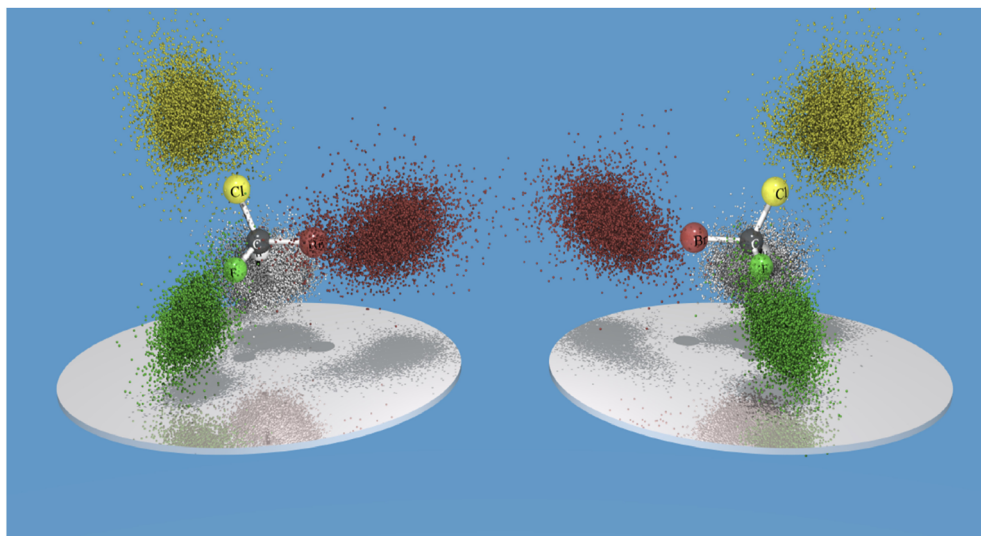
**ADVANCED
SCIENCE NEWS**

www.advancedsciencenews.com

annalen
der **physik**

www.ann-phys.org

Figure 33. Momentum–vector distribution of singly charged ionic fragments of the chiral CHBrClF molecule after laser ionization. White dot: H^+ ion; Black dot: C^+ ion; Green dots: F^+ ion; Yellow dots: Cl^+ ion; Red dots: Br^+ ions. Left: left handedness, right: right handedness (see text).[57,58a]
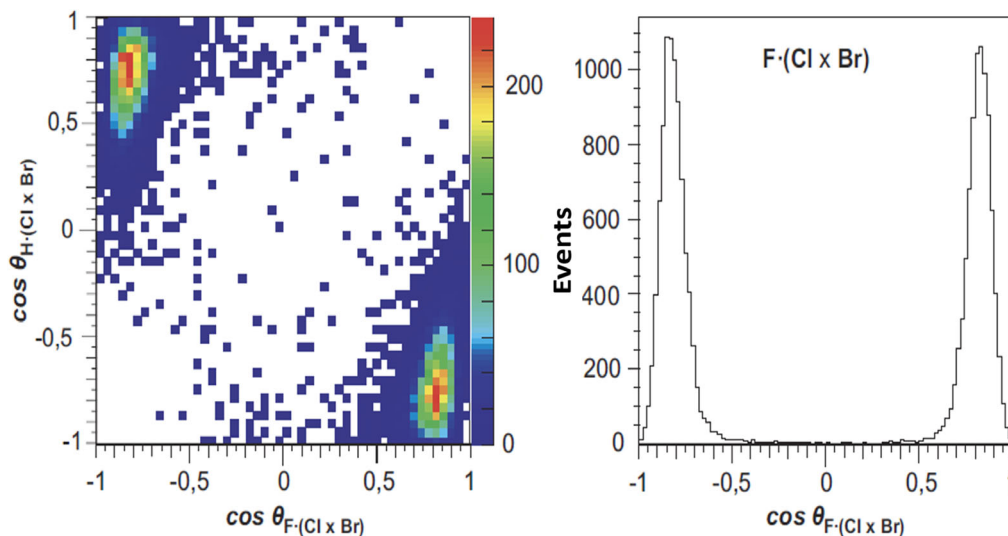

Figure 34. Measured handedness distribution as function of the chirality parameter $\cos \Theta_{F(Cl \times Br)} = p_F \bullet (p_{CL} \times p_{Br})/(|p_F| \bullet |p_{CL} \times p_{Br}|)$.[57,58]

distribution of the measured momentum vectors is shown of the multiple ionization of CHBrClF using a fs-laser in **Figure 33**. The Carbon ion momentum is fixed, the H ion is represented by the white dots, the F ion by the green dots, the Cl ion by the yellow dots and the Bromine ions by the red dots.

The multiple coincidence condition of 4 or five fragments reduces the background nearly to zero and allows to distinguish the enantiomers from a racemate, i.e., the experimenter can extract for each ionization event the handedness of the individual molecule. In **Figure 34** this unambiguous identification of the handedness by using C-REMI becomes obvious. Here the data are plotted as function of the chirality parameter

$$\cos \Theta_{F(Cl \times Br)} = p_F \bullet (p_{CL} \times p_{Br})/(|p_F| \bullet |p_{CL} \times p_{Br}|) \qquad (5)$$

3.13. Zeptosecond Time-Resolving Studies

In the recent past it has been demonstrated, that time-resolving experiments are possible without having a projectile source with corresponding timing properties, as, for example, in a laser pump–probe scheme. In some cases, the temporal evolution on atomic or molecular time scales can be deduced from other information obtained from the coincident detection of ions and electrons. This subsection will provide recent examples of such studies.[40,60,61]

Very recently, Grundmann et al.[61] investigated the following question employing a multiparticle coincidence approach: is an electron emitted simultaneously from all across a molecular orbital as it is released by photoionization, or is it first released from that region of its orbital that is "illuminated first" by the
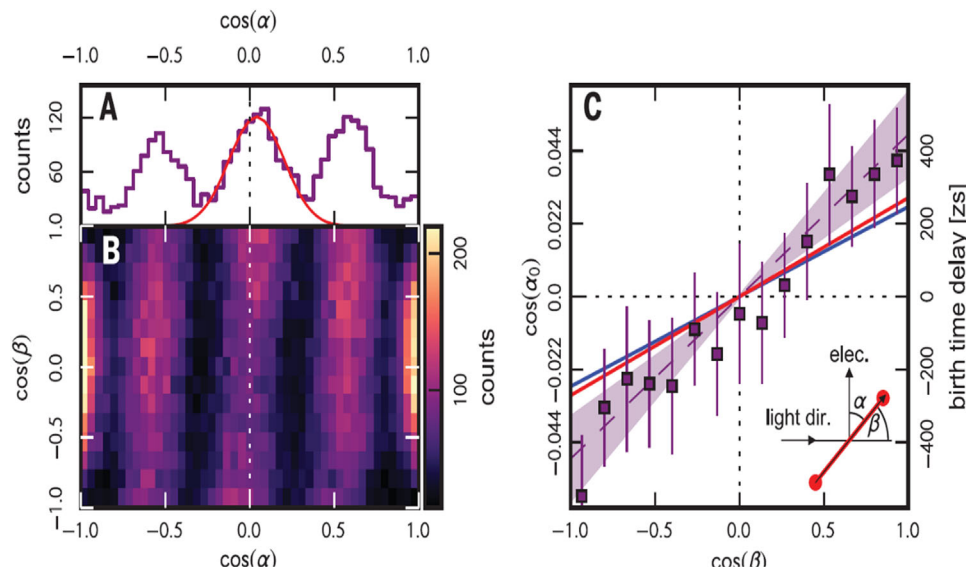
Figure 35. Left: interference pattern of photoelectrons emitted from H_2 horizontal axis emission angle of the electron with respect to the molecular axis, vertical axis: angle between the molecular axis and the light propagation direction. If the photoelectron wave would start at the same time from both centers of the molecule the central maximum would be at $\cos(\alpha) = 0$. From the observed shift the time delay between the emission from one to the other center can be deduced. Right: shift of the central interference fringe (left axis) and the corresponding time delay (right axis) as function of the molecular orientation to the light propagation axis. The blue line shows the expectation in case of a delay given by the speed of light, the red and dashed lines show the best linear fits throught the data. Adapted with permission.[61] Copyright 2020, AAAS.

photon? A H_2 molecule has been used as prototype test bench to answer this question (see **Figure 35**). Photoemission from a homonuclear molecule can be, due to the two-center nature of the molecule, intuitively regarded as a microscopic analog to scattering at a classical double slit. The photoelectron wave is emitted as a superposition from the "left" and the "right" atom of the molecule, which, indeed, causes Young-type interference patterns in the molecular frame angular emission distribution of the electron. Grundmann et al. showed that the molecular frame angular emission distribution changes subtly if the molecule is oriented along the photon propagation direction or perpendicular to it during the photoionization process. Within the double slit picture these changes are understandable: if the molecule is oriented perpendicular to the photon direction, the photon arrives at both nuclei of the molecule at the same time. However, if it oriented parallel to the propagation direction, one of the atom is hit prior to the second one. This delay in the arrival time can be modeled as a phase shift of the one of the emerging photoelectron waves, or, in the double slit picture, a phase shift in one of the two slits, which causes a measureable displacement of the double slit interference pattern. From this displacement a birth time delay of ≈250 zeptoseconds was resolved in the experiment, which nicely corresponds to the travel time of the photon along the molecule. The sensitivity of this approach is below a few 10 zs, despite employing synchrotron light pulses of >100 ps duration.

4. Conclusion

The C-REMI technique can be considered as the "Bubble Chamber" or "Time Projection Chamber" in atomic and molecular physics. Using the multicoincidence concept initially developed

in nuclear and high energy particle physics, a C-REMI can image the whole momentum space in a single-event quantum process even when the fragments have kinetic energies below a micro eV. Using ultracold targets in the gas phase and electromagnetic spectrometer designs with focusing conditions an excellent sub-atomic momentum resolution and a large multihit coincidence efficiency are obtained. Thus visualizing the complete dynamics in a single event the dynamical entanglement in many-particle systems can be explored.

The C-REMI is now a standard detection system in many fields of physics and chemistry and is used by many groups around the world. In several hundred laboratories worldwide C-REMI systems are operating, partially commercially purchased or self-made.[62] By using the C-REMI imaging technique many groups have produced numerous milestone discoveries. However, providing reference to all of these milestones in this review paper would exceed the purpose of this article. To present all benchmark results produced by the authors of this paper would also overshoot the capacity of this review. Thus only a small selection is presented here.

Appendix

A1) The standard sizes of atomic parameters, i.e., the "atomic units," are defined by the classical features of an electron in a hydrogen atom. The classical K-shell radius is $r_K = 5.29 \times 10^{-9}$ cm, which is used to define the atomic unit of length (a.u.). The classical electron velocity of the electron in the hydrogen K-shell is $v_K = 2.18 \times 10^8$ cm s^{-1}, which defines 1 a.u. of velocity. The classical momentum of the electron in the hydrogen K-shell is $p = m_e V_K = 1$ a.u. The atomic unit

of energy $E_{a.u.}$ is the mean potential energy of the H-K-shell electron (Hartree energy) $E_{a.u.} = 27.21$ eV. An atomic unit of time is defined by the ratio of the hydrogen K-shell radius divided by the corresponding electron velocity, or 5.29×10^{-9} cm divided by 2.1×10^{-8} cm s^{-1} yielding 24 as. Furthermore, the electron charge e and mass m_e are also set to 1 a.u. and hence $\bar{h}$ results to be 1 a.u., too.

A2) Subatomic resolution means <1 a.u., excellent resolution is then 0.01 a.u. or even better. Considering an electron a momentum resolution of 0.01 a.u. corresponds to about 1.4 meV energy resolution.

A3) One could name this kind of measurement a multielectron Compton scattering approach. The experimenter must ensure that like in traditional Compton scattering the remaining recoil ion acts as quasi spectator and does remain in its initial momentum state. This is generally the case if the ionization process is very short and photon-like.

A4) Heisenberg proposed in his famous paper[9] the concept of electron-position measurement using a so-called γ-microscope. He believed that the location of an electron at a given instant of time could be determined by scattering a γ-burst on the electron. He was convinced that even an ultimate position resolution in the 10^{-11} cm range could be achieved. From the subsequently measured locations and the time difference between the γ-bursts one could deduce then also information on the electron velocity, i.e., the electron momentum. He assumed that with the help of subsequent short wave-length γ-ray bursts one could visualize the trajectory of single electrons in atoms and molecules at given points in time. Thus making snapshots of the electron locations at subsequent moments in time the trajectory of these particles could be interpolated and thus information on the electron dynamics could be obtained. As discussed by Schmidt-Böcking et al.[7] this concept, however, can never work for a single electron at a given moment. There are several basic obstacles, which prevent such a kind of measurement. For example, the experimenter does not know, on which electron each detected γ-ray is scattered and how the momentum and location of that electron is then changed in each subsequent single γ-scattering process. Furthermore from one detected photon alone an electron position cannot be reduced. In addition there are a number of other unsolvable experimental difficulties[7,9] like the experimental creation of such short γ-bursts with the required intensity and burst rate. As discussed Schmidt-Böcking et al.[7] locations of electrons at a given moment in a single scattering event inside atoms or molecules or inside the reaction zone can never be measured with subatomic position resolution. A subatomic position resolution in a single scattering event is prevented by the basic laws of physics.[7] The experimenter might be able to position in the preparation stage of the measurement a target atom or projectile with about 1 a.u. accuracy, but because of the uncertainty relation in preparing this location the quantum particles can never be brought at rest. Thus the particle is randomly moving during the time of measurement (duration femto- to nanoseconds) yielding large uncertainties in a position measurement. Positions are not conserved with varying time.

Conflict of Interest

The authors declare no conflict of interest.

[1] a) J. Ullrich, R. Dörner, V. Mergel, O. Jagutzki, L. Spielberger, H. Schmidt-Böcking, *Comments At. Mol. Phys.* **1994**, *30*, 285; b) J. Ullrich, R. Dörner, H. Schmidt-Böcking, *Am. Inst. Phys.* **1996**, 12; c) R. Moshammer, M. Unverzagt, W. Schmitt, J. Ullrich, H. Schmidt-Böcking, *Nucl. Instrum. Methods, Sect. B* **1996**, *108*, 425; d) J. Ullrich, R. Moshammer, R. Dörner, O. Jagutzki, V. Mergel, H. Schmidt-Böcking, L. Spielberger, *J. Phys. B: At., Mol. Opt. Phys.* **1997**, *30*, 2917; e) J. Ullrich, W. Schmitt, R. Dörner, O. Jagutzki, V. Mergel, R. Moshammer, H. Schmidt-Böcking, L. Spielberger, M. Unverzagt, R. E. Olson, in *Recoil Ion Momentum Spectroscopy, Photonic, Electronic and Atomic Collisions*, (Eds: F. Aumayr, et al.) World Scientific, New York **1997**, p. 421; f) J. Ullrich, R. Moshammer, A. Dorn, R. Dörner, L. P. H. Schmidt, H. Schmidt-Böcking, *Rep. Prog. Phys.* **2003**, *66*, 1463.

[2] a) R. Dörner, V. Mergel, H. Bräuning, M. Achler, T. Weber, K.h. Khayyat, O. Jagutzki, L. Spielberger, J. Ullrich, R. Moshammer, Y. Azuma, M. H. Prior, C. L. Cocke, H. Schmidt-Böcking, in *Proc. the AIP Conf. on Atomic Processes in Plasmas* (Eds: E. Oks, M. Pindzola), AIP, New York **1998**, p. 443; b) R. Dörner, V. Mergel, O. Jagutzki, L. Spielberger, J. Ullrich, R. Moshammer, H. Schmidt-Böcking, *Phys. Rep.* **2000**, *330*, 95; c) R. Dörner, T.h. Weber, M. Weckenbrock, A. Staudte, M. Hattass, R. Moshammer, J. Ullrich, H. Schmidt-Böcking, in *Multiple Ionization in Strong Laser Fields Advances in Atomic and Molecular Physics* (Eds: B. Bederson, H. Walther). Academic Press, MA **2002**, p. 48.

[3] T. Jahnke, et al., in *Molecular Beams in Physics and Chemistry*, (Eds: B. Friedrich, H. Schmidt-Böcking). Springer International Publishing, New York **2021**.

[4] a) N. Bohr, *Philos. Mag.* **1913**, *26*, 1; b) *Philos. Mag.* **1913**, *26*, 476; c) *Philos. Mag.* **1913**, *26*, 857.

[5] a) W. Heisenberg, *Z. Phys.* **1925**, *33*, 879; b) M. Born, P. Jordan, *Z. Phys.* **1925**, *34*, 858; c) M. Born, W. Heisenberg, P. Jordan, *Z. Phys.* **1926**, *35*, 557.

[6] E. Schrödinger, *Ann. Phys.* **1926**, *79*, 361.

[7] H. Schmidt-Böcking, S. Eckart, H. J. Lüdde, G. Gruber, T. Jahnke, in *Molecular Beams in Physics and Chemistry* (Eds: B. Friedrich, H. Schmidt-Böcking), Springer International Publishing, New York **2021**, Chapter 12, p. 223.

[8] J. Burgdörfer, C. Lemmel, X. Tong, Invited Lecture at ICPEAC, January **2019**, arXiv:2001.02900v1.

[9] W. Heisenberg, *Z. Phys.* **1927**, *43*, 172.

[10] a) U. Buck, M. Düker, H. Pauly, D. Rust, *Proc. of the IV Int. Symp. on Molecular Beams* **1974**, p. 70; b) H. Haberland, U. Buck, M. Tolle, *Rev. Sci. Instrum.* **1985**, *56*, 1712.

[11] D. Akoury, *Diploma* **2008**.

[12] C. Janke, *Ph.D. Thesis*, University Frankfurt, Germany **2020**.

[13] a) M. van der Poel, C. V. Nielsen, M. A. Gearba, N. Andersen, *Phys. Rev. Lett.* **2001**, *87*, 123201; b) J. W. Turkstra, R. Hoekstra, S. Knoop, D. Meyer, R. Morgenstern, R. E. Olson, *Phys. Rev. Lett.* **2001**, *87*, 123; c) X. Flechard, H. Nguyen, E. Wells, I. Ben-Itzhak, B. D. DePaola, *Phys. Rev. Lett.* **2001**, *87*, 123203.

[14] a) O. Jagutzki, V. Mergel, K. Ullmann-Pfleger, L. Spielberger, U. Meyer, R. Doerner, H. W. Schmidt-Boecking, *Proc SPIE* **1998**, *3438*, 322; b) C. Janke, *Ph.D. Thesis*, University Frankfurt, Germany **2020**; c) K. Fehre, D. Trojanowskaja, J. Gatzke, M. Kunitski, F. Trinter, S. Zeller, L. Ph. H. Schmidt, J. Stohner, R. Berger, A. Czasch, O. Jagutzki, T. Jahnke, R. Dörner, M. S. Schöffler, *Rev. Sci. Instrum.* **2018**, *89*, 045112.

[15] F. Trinter, personal communication.

[16] a) R. Moshammer, J. Ullrich, M. Unverzagt, W. Schmidt, P. Jardin, R. E. Olson, R. Mann, R. Dörner, V. V Mergel, U. Buck, H. Schmidt-Böcking, *Phys. Rev. Lett.* **1994**, *73*, 3371; b) J. Ullrich, R. Doerner, V. Mergel, O. Jagutzki, L. Spielberger, H. Schmidt-Boecking, *Comments At. Mol. Phys.* **1994**, *30*, 285.

[17] a) M. Unverzagt, R. Moshammer, W. Schmitt, R. E. Olson, P. Jardin, V. Mergel, J. Ullrich, H. Schmidt-Böcking, *Phys. Rev. Lett.* **1996**, *76*, 1043; b) R. Moshammer, J. Ullrich, H. Kollmus, W. Schmitt, M. Unverzagt, O. Jagutzki, V. V Mergel, H. Schmidt-Böcking, R. Mann, C. J. Woods, R. E. Olson, *Phys. Rev. Lett.* **1996**, *77*, 1242; c) R. Moshammer, J. Ullrich, H. Kollmus, W. Schmitt, M. Unverzagt, H. Schmidt-Böcking, C. J. Wood, R. E. Olson, *Phys. Rev. A* **1997**, *56*, 1351; d) R. Moshammer, W. Schmitt, J. Ullrich, H. Kollmus, A. Cassimi, R. Dorner, O. Jagutzki, R. Mann, R. E. Olson, H. T. Prinz, H. Schmidt-Bocking, L. Spielberger, *Phys. Rev. Lett.* **1997**, *79*, 3621.

[18] a) G. Tanner, K. Richter, J. M. Rost, *Rev. Mod. Phys.* **2000**, *72*, 497; b) T. Kinoshita, *Phys. Rev.* **1959**, *115*, 366; c) G. W. F. Drake, in *Long range Casimir Forces* (Eds: F. S. Levin, D. A. Micha) Plenum, New York **1994**, p. 107.

[19] a) V. Mergel, *Ph.D. Thesis*, Universität Frankfurt, **1996**; b) V. Mergel, R. Dörner, M. Achler, K.h. Khayyat, S. Lencinas, J. Euler, O. Jagutzki, S. Nüttgens, M. Unverzagt, L. Spielberger, W. Wu, R. Ali, J. Ullrich, H. Cederquist, A. Salin, C. J. Wood, R. E. Olson, Dž. Belkić, C. L. Cocke, H. Schmidt-Böcking, *Phys. Rev. Lett.* **1997**, *79*, 387; c) V. Mergel, et al., *Phys. Rev. Lett.* **2001**, *86*, 2257; d) V. Mergel, personal communication.

[20] a) H. Schmidt-Böcking, V. Mergel, R. Dörner, C. L. Cocke, O. Jagutzki, L. Schmidt, T h. Weber, H. J. Lüdde, E. Weigold, J. Berakdar, H. Cederquist, H. T. Schmidt, R. Schuch, A. S. Kheifets, *Europhys. Lett.* **2003**, *62*, 477; b) A. Kheifets, personal communication.

[21] a) M. Schöffler, A. L. Godunov, C. T. Whelan, H. R. J. Walters, V. S. Schipakov, V. Mergel, R. Dörner, O. Jagutzki, L. Ph. H. Schmidt, J. Titze, E. Weigold, H. Schmidt-Böcking, *J. Phys. B: At., Mol. Opt.* **2005**, *38*, L123; b) A. L. Godunov, C. T. Whelan, H. R. J. Walters, V. S. Schipakov, M. Schöffler, V. Mergel, R. Dörner, O. Jagutzki, L. Ph. H. Schmidt, J. Titze, H. Schmidt-Böcking, *Phys. Rev. A* **2005**, *71*, 052712; c) H. Schmidt-Bocking, personal communication.

[22] M. S. Schöffler, *Ph.D. Dissertation*, Universität Frankfurt, Frankfurt **2006**.

[23] a) M. S. Schöffler, O. Chuluunbaatar, S. Houamer, A. Galstyan, J. N. Titze, L. Ph. H. Schmidt, T. Jahnke, H. Schmidt-Böcking, R. Dörner, Y. U. V. Popov, A. A. Gusev, C. Dal Cappello, *Phys. Rev. A* **2013**, *88*, 042710; b) M. S. Schöffler, H.-K. Kim, O. Chuluunbaatar, S. Houamer, A. G. Galstyan, J. N. Titze, T. Jahnke, L. Ph. H. Schmidt, H. Schmidt-Böcking, R. Dörner, Yu. V. Popov, A. A. Bulychev, *Phys. Rev. A* **2014**, *89*, 032707; c) M. S. Schöffler, C. Stuck, M. Waitz, F. Trinter, T. Jahnke, U. Lenz, M. Jones, A. Belkacem, A. Landers, M. S. Pindzola, C. L. Cocke, J. Colgan, A. Kheifets, I. Bray, H. Schmidt-Böcking, R. Dörner, Th. Weber, *Phys. Rev. Lett.* **2013**, *111*, 013003; d) S. Grundmann, F. Trinter, A. W. Bray, S. Eckart, J. Rist, G. Kastirke, D. Metz, S. Klumpp, J. Viefhaus, L. Ph. H. Schmidt, J. B. Williams, R. Dörner, T. Jahnke, M. S. Schöffler, A. S. Kheifets, *Phys. Rev. Lett.* **2018**, *121*, 173003.

[24] L. H. Thomas, *Proc. R. Soc. London, Ser. A* **1927**, *114*, 561.

[25] a) C. Held, *Die Bohr-Einstein-Debatte: Quantenmechanik und physikalische Wirklichkeit, Schöningh*, Paderborn, Germany **1998**; b) N. Bohr, *The Value of Knowledge: A Miniature Library of Philosophy. Marxists Internet Archive*, Retrieved 2010-08-30. From Albert Einstein: Philosopher-Scientist, 1949, Cambridge University Press, New York **1949**. Niels Bohr's report of conversations with Einstein. https://en.wikipedia.org/wiki/Bohr%E2%80%93Einstein_debates. Footnote to [25]: Bohr replied to Einstein that the experimenter is in the preparation of the slits initial state limited by the uncertainty relationship. He can either prepare the slit with a narrow initial momentum distribution such that he could measure the momentum transfer but then the width in position would lead to a loss of coherence and a loss of the interference. Alternatively, the experimenter could fix the location of the slit on the price of accepting a large initial momentum uncertainty which would prohibit the inference of the pathways but lead to a high contrast interference pattern.

[26] L. Ph. H. Schmidt, S. Schössler, F. Afaneh, M. Schöffler, K. E. Stiebing, H. Schmidt-Böcking, R. Dörner, *Phys. Rev. Lett.* **2008**, *101*, 173202.

[27] A. Niehaus, *Phys. Rep.* **1990**, *149*, 186.

[28] a) R. Dörner, H. Khemliche, M. H. Prior, C. L. Cocke, J. A. Gary, R. E. Olson, V. Mergel, J. Ullrich, H. Schmidt-Böcking, *Phys. Rev. Lett.* **77**, 4520; b) M. A. Abdallah, C. L. Cocke, W. Wolff, H. Wolf, S. D. Kravis, M. Stöckli, E. Kamber, *Phys. Rev. Lett.* **1998**, *81*, 3627.

[29] a) L. Ph. H. Schmidt, C. Goihl, D. Metz, H. Schmidt-Böcking, R. Dörner, S. Yu. Ovchinnikov, J. H. Macek, D. R. Schultz, *Phys. Rev. Lett.* **2014**, *112*, 083201; b) L. Ph. H. Schmidt, M. Schöffler, C. Goihl, T. Jahnke, H. Schmidt-Böcking, R. Dörner, *Phys. Rev. A 94*, 052701.

[30] a) L. Ph. H. Schmidt, T. Jahnke, A. Czasch, M. Schöffler, H. Schmidt-Böcking, R. Dörner, *Phys. Rev. Lett. 108*, 073202; b) L. Schmidt, personal communication.

[31] a) L. Spielberger, Ph.D. Dissertation, Universität Frankfurt, New York **1996**; b) L. Spielberger, O. Jagutzki, R. Dörner, J. Ullrich, U. Meyer, V. V Mergel, M. Unverzagt, M. Damrau, T. Vogt, I. I Ali, K. Khayyat, D. Bahr, H. G. Schmidt, R. Frahm, H. Schmidt-Böcking, *Phys. Rev. Lett.* **1995**, *74*, 4615; c) L. Spielberger, H. Bräuning, A. Muthig, J. Z. Tang, J. Wang, Y. Qiu, R. Dörner, O. Jagutzki, Th. Tschentscher, V. Honkimäki, V. Mergel, M. Achler, T.h. Weber, K.h. Khayyat, J. Burgdörfer, J. McGuire, H. Schmidt-Böcking, *Phys. Rev. A* **1999**, *59*, 371; d) L. Spielberger, personal communication.

[32] B. Krässig, R. W. Dunford, D. S. Gemmell, S. Hasegawa, E. P. Kanter, H. Schmidt-Böcking, W. Schmitt, S. H. Southworth, Th. Weber, L. Young, *Phys. Rev. Lett.* **1999**, *83*.

[33] P. M. Bergstrom Jr., K. Hino, J. Macek, *Phys. Rev.* **1995**, *51*, 3044.

[34] a) B. S. B. Walker, L. F. DiMauro, P. Agostini, K. J. Schafer, K. C. Kulander, *Phys. Rev. Lett.* **1994**, *73*, 1994; b) B. Walker, B. Sheehy, K. C. Kulander, L. F. DiMauro, *Phys. Rev. Lett.* **1996**, *77*, 5031.

[35] a) P. B. Corkum, *Phys. Rev. Lett.* **1993**, *71*, 1994; b) K. C. Kulander, J. Cooper, K. J. Schafer, *Phys. Rev. A* **1995**, *51*, 561.

[36] a) R. Moshammer, J. Ullrich, B. Feuerstein, D. Fischer, A. Dorn, C. D. Schröter, J. R. Crespo Lopez-Urrutia, C. Hoehr, H. Rottke, C. Trump, M. Wittmann, G. Korn, W. Sandner, *Phys. Rev. Lett.* **2003**, *91*, 113002; b) R. Moshammer, J. Ullrich, B. Feuerstein, D. Fischer, A. Dorn, C. D. Schröter, J. R. Crespo López-Urrutia, C. Höhr, H. Rottke, C. Trump, M. Wittmann, G. Korn, K. Hoffmann, W. Sandner, *J. Phys. B* **2003**, 36.

[37] a) T. Weber, M. Weckenbrock, A. Staudte, M. Hattass, L. Spielberger, O. Jagutzki, V. Mergel, H. Bocking, G. Urbasch, H. Giessen, H. Brauning, C. Cocke, M. Prior, R. Doerner, *Opt. Express* **2001**, *8*, 368; b) T. Weber, M. Weckenbrock, A. Staudte, L. Spielberger, O. Jagutzki, V. V Mergel, F. Afaneh, G. Urbasch, M. Vollmer, H. Giessen, R. Dorner, *Phys. Rev. Lett.* **2000**, *84*, 443; c) T. Weber, H. Giessen, M. Weckenbrock, G. Urbasch, A. Staudte, L. Spielberger, O. Jagutzki, V. Mergel, M. Vollmer, R. Dorner, *Nature* **2000**, *405*, 658; d) T. Weber, personal communication.

[38] a) M. Weckenbrock, A. Becker, A. Staudte, S. Kammer, M. Smolarski, V. R. Bhardwaj, D. M. Rayner, D. M. Villeneuve, P. B. Corkum, R. Dörner, *Phys. Rev. Lett.* **2003**, *91*, 123004; b) M. Weckenbrock, D. Zeidler, A. Staudte, Th. Weber, M. Schöffler, M. Meckel, S. Kammer, M. Smolarski, O. Jagutzki, V. R. Bhardwaj, D. M. Rayner, D. M. Villeneuve, P. B. Corkum, R. Dörner, *Phys. Rev. Lett.* **2004**, *92*, 213002.

[39] F. Trinter, L. Ph. H. Schmidt, T. Jahnke, M. S. Schöffler, O. Jagutzki, A. Czasch, J. Lower, T. A. Isaev, R. Berger, A. L. Landers, Th. Weber, R. Dörner, H. Schmidt-Böcking, *Mol. Phys.* **2012**, *110*, 1863.

[40] M. S. Schöffler, J. Titze, N. Petridis, T. Jahnke, K. Cole, L. Ph. H. Schmidt, A. Czasch, D. Akoury, O. Jagutzki, J. B. Williams, N. A. Cherepkov, S. K. Semenov, C. W. McCurdy, T. N. Rescigno, C. L. Cocke, T. Osipov, S. Lee, M. H. Prior, A. Belkacem, A. L. Landers, H. Schmidt-Böcking, Th. Weber, R. Dörner, *Science* **2008**, *320*, 920.

[41] L. S. Cederbaum, J. Zobeley, F. Tarantelli, *Phys. Rev. Lett.* **1997**, *79*, 4778.

[42] S. Marburger, O. Kugeler, U. Hergenhahn, T. Möller, *Phys. Rev. Lett.* **2003**, *90*, 203401.

[43] a) T. Jahnke, A. Czasch, M. S. Schöffler, S. Schössler, A. Knapp, M. Käsz, J. Titze, C. Wimmer, K. Kreidi, R. E. Grisenti, A. Staudte, O. Jagutzki, U. Hergenhahn, H. Schmidt-Böcking, R. Dörner, *Phys. Rev. Lett.* **2004**, *93*, 163401; b) T. Jahnke, *Ph.D. Dissertation*, Universität Frankfurt, Germany **2005**; c) T. Jahnke, personal communication.

[44] F. Trinter, J. B. Williams, M. Weller, M. Waitz, M. Pitzer, J. Voigtsberger, C. Schober, G. Kastirke, C. Müller, C. Goihl, P. Burzynski, F. Wiegandt, R. Wallauer, A. Kalinin, L. Ph. H. Schmidt, M. S. Schöffler, Y.-C. Chiang, K. Gokhberg, T. Jahnke, R. Dörner, *Phys. Rev. Lett.* **2013**, *111*, 233004.

[45] B. Najjari, A. B. Voitkiv, C. Müller, *Phys. Rev. Lett.* **2010**, *105*, 153002.

[46] T. Jahnke, A. Czasch, M. Schöffler, S. Schössler, M. Käsz, J. Titze, K. Kreidi, R. E. Grisenti, A. Staudte, O. Jagutzki, L. Ph. H. Schmidt, Th. Weber, H. Schmidt-Böcking, K. Ueda, R. Dörner, *Phys. Rev. Lett.* **2007**, *99*, 153401.

[47] K. Kreidi, P.h V. Demekhin, T. Jahnke, T.h Weber, T. Havermeier, X.-J. Liu, Y. Morisita, S. Schössler, L. Ph. H. Schmidt, M. Schöffler, M. Odenweller, N. Neumann, L. Foucar, J. Titze, B. Ulrich, F. Sturm, C. Stuck, R. Wallauer, S. Voss, I. Lauter, H. K. Kim, M. Rudloff, H. Fukuzawa, G. Prümper, N. Saito, K. Ueda, A. Czasch, O. Jagutzki, H. Schmidt-Böcking, S. Scheit, L. S. Cederbaum, R. Dörner, *Phys. Rev. Lett.* **2009**, *103*, 033001.

[48] N. Sisourat, H. Sann, N. V. Kryzhevoi, P. Kolorenč, T. Havermeier, F. Sturm, T. Jahnke, H.-K. Kim, R. Dörner, L. S. Cederbaum, *Phys. Rev. Lett.* **2010**, *105*, 173401.

[49] T. Havermeier, T. Jahnke, K. Kreidi, R. Wallauer, S. Voss, M. Schöffler, S. Schössler, L. Foucar, N. Neumann, J. Titze, H. Sann, M. Kühnel, J. Voigtsberger, J. H. Morilla, W. Schöllkopf, H. Schmidt-Böcking, R. E. Grisenti, R. Dörner, *Phys. Rev. Lett.* **2010**, *104*, 133401.

[50] a) J. Titze, M. S. Schöffler, H.-K. Kim, F. Trinter, M. Waitz, J. Voigtsberger, N. Neumann, B. Ulrich, K. Kreidi, R. Wallauer, M. Odenweller, T. Havermeier, S. Schössler, M. Meckel, L. Foucar, T. Jahnke, A. Czasch, L. Ph. H. Schmidt, O. Jagutzki, R. E. Grisenti, H. Schmidt-Böcking, H. J. Lüdde, R. Dörner, *Phys. Rev. Lett.* **2011**, *106*, 033201; b) T. Jahnke, U. Hergenhahn, B. Winter, R. Dörner, U. Frühling, Ph. V. Demekhin, K. Gokhberg, L. S. Cederbaum, A. Ehresmann, A. Knie, A. Dreuw, *Chem. Rev.* **2020**, *120*, 11295.

[51] T. Ergler, A. Rudenko, B. Feuerstein, K. Zrost, C. D. Schröter, R. Moshammer, J. Ullrich, *Phys. Rev. Lett.* **2006**, *97*, 193001.

[52] a) M. Kunitski, Q. Guan, H. Maschkiwitz, J. Hahnenbruch, S. Eckart, S. Zeller, A. Kalinin, M. Schöffler, L. Ph. H. Schmidt, T. Jahnke, D. Blume, R. Dörner, *Nat. Phys.* **2020**; b) M. Kunitski, personal communication.

[53] R. W. Robinet, *Phys. Rep.* **2004**, *392*, 1.

[54] V. Efimov, *Phys. Lett. B* **1970**, *33*, 563.

[55] M. Kunitski, S. Zeller, J. Voigtsberger, A. Kalinin, L. P. H. Schmidt, M. Schöffler, A. Czasch, W. Schöllkopf, R. E. Grisenti, T. Jahnke, D. Blume, R. Dörner, *Science* **2015**, *348*, 551.

[56] W. Schöllkopf, J. P. Toennies, *Science* **1994**, *266*, 1345.

[57] M. Pitzer, *Ph.D. Dissertation*, Universität Frankfurt, Germany **2015**.

[58] a) M. Pitzer, M. Kunitski, A. S. Johnson, T. Jahnke, H. Sann, F. Sturm, L. Ph. H. Schmidt, H. Schmidt-Böcking, R. Dörner, J. Stohner, J. Kiedrowski, M. Reggelin, S. Marquardt, A. Schießer, R. Berger, M. S. Schöffler, *Science* **2013**, *341*, 1096; b) M. Pitzer, G. Kastirke, P. Burzynski, M. Weller, D. Metz, J. Neff, M. Waitz, F. Trinter, L. Ph. H. Schmidt, J. B. Williams, T. Jahnke, H. Schmidt-Böcking, R. Berger, R. Dörner, M. Schöffler, *J. Phys. B: At., Mol. Opt.* **2016**, *49*, 234001; c) M. Pitzer, G. Kastirke, M. Kunitski, T. Jahnke, T. Bauer, C. Goihl, F. Trinter, C. Schober, K. Henrichs, J. Becht, S. Zeller, H. Gassert, M. Waitz, A. Kuhlins, H. Sann, F. Sturm, F. Wiegandt, R. Wallauer, L. Ph. H. Schmidt, A. S. Johnson, M. Mazenauer, B. Spenger, S. Marquardt, S. Marquardt, H. Schmidt-Böcking, J. Stohner, R. Dörner, M. Schöffler, R. Berger, *Chem. Phys. Chem.* **2016**, *17*, 2465; d) M. Pitzer, *J. Phys. B: At., Mol. Opt.* **2017**, *50*, 153001; e) M. Pitzer, K. Fehre, M. Kunitski, T. Jahnke, L. Schmidt, H. Schmidt-Böcking, R. Dörner, M. Schöffler, *JoVE - J. Visualized Exp.* **2017**, *126*, 56062; f) M. Pitzer, P. Martin, B. Robert, S. Jürgen, D. Reinhard, S. Markus, *Chimia* **2018**, *72*, 384; g) M. Pitzer, personal communication.

[59] a) K. Fehre, S. Eckart, M. Kunitski, M. Pitzer, S. Zeller, C. Janke, D. Trabert, J. Rist, M. Weller, A. Hartung, L. Ph. H. Schmidt, T. Jahnke, R. Berger, R. Dörner, M. S. Schöffler, *Sci. Adv.* **2019**, 3; b) K. Fehre, S. Eckart, M. Kunitski, M. Pitzer, S. Zeller, C. Janke, D. Trabert, J. Rist, M. Weller, A. Hartung, L. Ph. H. Schmidt, T. Jahnke, R. Berger, R. Dörner, M. S. Schöffler, *Sci. Adv.* **2019**, *5*, 3.

[60] H. Sann, T. Havermeier, C. Müller, H.-K. Kim, F. Trinter, M. Waitz, J. Voigtsberger, F. Sturm, T. Bauer, R. Wallauer, D. Schneider, M. Weller, C. Goihl, J. Tross, K. Cole, J. Wu, M. S. Schöffler, H. Schmidt-Böcking, T. Jahnke, M. Simon, R. Dörner, *Phys. Rev. Lett.* **2016**, *117*, 243002.

[61] a) S. Grundmann, D. Trabert, K. Fehre, N. Strenger, A. Pier, L. Kaiser, M. Kircher, M. Weller, S. Eckart, L. Ph. H. Schmidt, F. Trinter, T. Jahnke, M. S. Schöffler, R. Dörner, *Science* **2020**, *370*, 339; b) S. Grundmann, personal communication.

[62] http://roentdek.com/

In a long time collaboration beginning in the late seventies until now the four authors Horst Schmidt-Böcking, Joachim Ullrich, Reinhard Dörner, and Charles Lewis Cocke have developed together with their group members the in this paper described COLTRIMS reaction microscope. This multi-coincidence high resolution momentum imaging device can visualize inner atomic and molecular dynamics on the one atto-second scale.

Horst Schmidt-Böcking obtained his Ph.D. in nuclear physics at the University Heidelberg. From 1982 till 2004 he was professor for experimental atomic and molecular physics at the University Frankfurt. He retired in 2004. For his contributions to experimental quantum physics he has received among other awards in 1991 the Max-Planck-Forschungspreis together with C. L. Cocke, in 2008 the Davisson-Germer Award of the American Physical Society, and in 2010 the Stern-Gerlach Medal of the German Physical Society. After his retirement he has published several books on the life and work of Otto Stern.

Joachim Ullrich obtained his Ph.D. in 1987 at the University Frankfurt. From 1997 till 2001 he was professor for atomic and molecular physics at the University Freiburg, from 2001 till 2012 professor for atomic and molecular physics at the University Heidelberg and director of the Max-Planck-Institut für Kernphysik at Heidelberg, and from 2012 until now president of the Physikalisch-Technische Bundesanstalt in Braunschweig. For his contributions to experimental quantum physics he has received among other awards in 1999 the Leibniz Preis of the "Deutsche Forschungsgemeinschaft," in 2004 the David Bates Medal of the London Institute of Physics, in 2006 the Philip Morris Forschungspreis, and in 2021 the Stern-Gerlach Medal of the German Physical society.

Reinhard Dörner is since 2002 until now professor for experimental atomic and molecular physics at the University Frankfurt. In 1991 he obtained his Ph.D. at the University Frankfurt. From 1995 until 1998 he was Feodor Lynen and Heisenberg Fellow at LBNL in Berkeley. For his contributions to experimental quantum physics he has received among other awards in 1998 the Adolph Messer Wissenschaftspreis, in 2015 the Robert-Wichard-Pohl Preis of the German Physical Society, and in 2016 the Helmholtz Preis.

Charles Lewis Cocke obtained his Ph.D. in 1967 at the California Institute of Technology. Since 1969 until his retirement in 2011 he was professor (since 1993 distinguished professor) for experimental atomic and molecular physics at Kansas State University in Manhattan/KS. For his contributions to experimental quantum physics he has received among other awards in 1991 the Senior Alexander von Humboldt Award and the Max-Planck Forschungspreis, in 2003 the Olin K. Petefish (Higuchi) Award of the KSU, in 2005 an honorary doctor degree of the University Frankfurt and in 2006 the Davisson-Germer-Award of the American Physical Society.